Article

Cell Reports

Skeletal Muscle-Specific Methyltransferase METTL21C Trimethylates p97 and Regulates Autophagy-Associated Protein Breakdown

Graphical Abstract

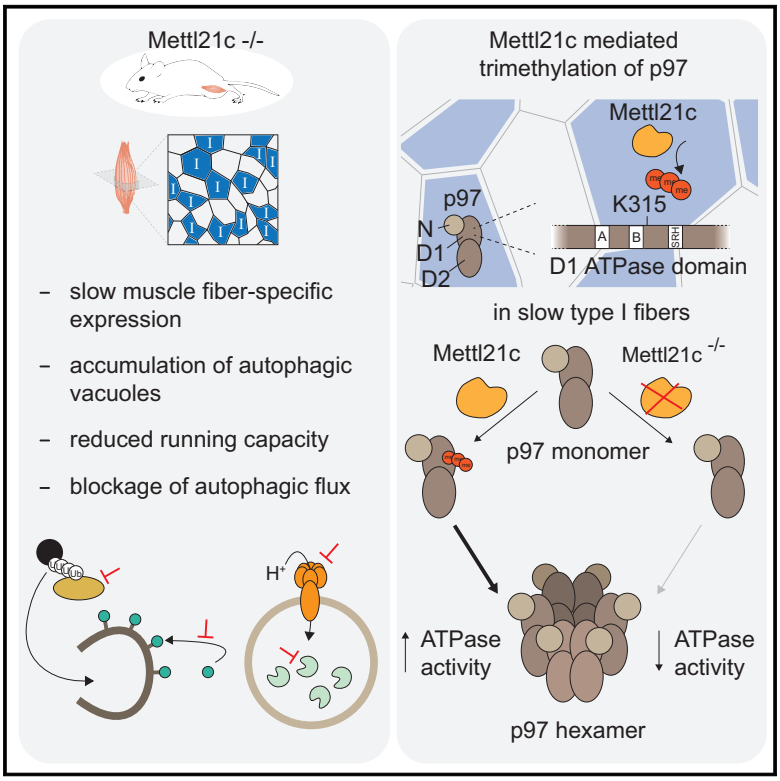

Highlights

- METTL21C is exclusively expressed in slow MYH7-positive skeletal muscle fibers
- *Mettl21c*$^{-/-}$ mice present muscle weakness and accumulate autophagic vacuoles
- Denervation-induced atrophy reveals dysregulated autophagy in *Mettl21c*$^{-/-}$ mice
- p97 hexamer assembly and ATPase activity are reduced in *Mettl21c*$^{-/-}$ muscles

Authors

Janica Lea Wiederstein, Hendrik Nolte, Stefan Günther, ..., Thomas Braun, Soraya Hölper, Marcus Krüger

Correspondence

soraya.hoelper@sanofi.com (S.H.), marcus.krueger@uni-koeln.de (M.K.)

In Brief

Wiederstein et al. describe the skeletal muscle methyltransferase Mettl21c. They found that ablation of Mettl21c in mice results in muscle weakness and disturbance of the protein degradation machinery. Those changes are hallmarks of multisystem proteinopathies. They demonstrate that Mettl21c modulates p97 activity, which is frequently mutated in human patients with muscle weakness.

Data and Software Availability

PXD008145

Wiederstein et al., 2018, Cell Reports *23*, 1342–1356
May 1, 2018
https://doi.org/10.1016/j.celrep.2018.03.136

CellPress

OPEN ACCESS
CellPress

Cell Reports
Article

Skeletal Muscle-Specific Methyltransferase METTL21C Trimethylates p97 and Regulates Autophagy-Associated Protein Breakdown

Janica Lea Wiederstein,[1] Hendrik Nolte,[1] Stefan Günther,[2] Tanja Piller,[3] Martina Baraldo,[4] Sawa Kostin,[2] Wilhelm Bloch,[5] Natalie Schindler,[6] Marco Sandri,[4] Bert Blaauw,[4] Thomas Braun,[2] Soraya Hölper,[7,*] and Marcus Krüger[1,8,9,*]

[1]Institute for Genetics, Cologne Excellence Cluster on Cellular Stress Responses in Aging-Associated Diseases (CECAD), Cologne, Germany
[2]Max Planck Institute for Heart and Lung Research, Ludwigstr. 43, 61231 Bad Nauheim, Germany
[3]Institute of Biochemistry II, Goethe University Medical School, 60590 Frankfurt, Germany
[4]Venetian Institute of Molecular Medicine (VIMM), Department of Biomedical Sciences Padova, University of Padova, Italy
[5]Department of Molecular and Cellular Sport Medicine, Institute of Sport Medicine and Cardiovascular Research, German Sport University, Cologne, Germany
[6]Institut für Entwicklungsbiologie und Neurobiologie (IDN), Fachbereich Biologie (FB 10), Johannes Gutenberg University (JGU), Mainz, Germany, c/o Institute of Molecular Biology gGmbH (IMB), Mainz, Germany
[7]Sanofi-Aventis Deutschland GmbH, Biologics Research, Protein Therapeutics, Industriepark Höchst, 65926 Frankfurt, Germany
[8]Center for Molecular Medicine (CMMC), University of Cologne, 50931 Cologne, Germany
[9]Lead Contact
*Correspondence: soraya.hoelper@sanofi.com (S.H.), marcus.krueger@uni-koeln.de (M.K.)
https://doi.org/10.1016/j.celrep.2018.03.136

SUMMARY

Protein aggregates and cytoplasmic vacuolization are major hallmarks of multisystem proteinopathies (MSPs) that lead to muscle weakness. Here, we identify METTL21C as a skeletal muscle-specific lysine methyltransferase. Insertion of a β-galactosidase cassette into the *Mettl21c* mouse locus revealed that METTL21C is specifically expressed in MYH7-positive skeletal muscle fibers. Ablation of the *Mettl21c* gene reduced endurance capacity and led to age-dependent accumulation of autophagic vacuoles in skeletal muscle. Denervation-induced muscle atrophy highlighted further impairments of autophagy-related proteins, including LC3, p62, and cathepsins, in *Mettl21c*$^{-/-}$ muscles. In addition, we demonstrate that METTL21C interacts with the ATPase p97 (VCP), which is mutated in various human MSP conditions. We reveal that METTL21C trimethylates p97 on the Lys315 residue and found that loss of this modification reduced p97 hexamer formation and ATPase activity *in vivo*. We conclude that the methyltransferase METTL21C is an important modulator of protein degradation in skeletal muscle under both normal and enhanced protein breakdown conditions.

INTRODUCTION

Balanced regulation of protein synthesis and breakdown is crucial to maintain skeletal muscle function (Cohen et al., 2015; Schiaffino and Reggiani, 2011). Proteolysis is primarily mediated by the ubiquitin-proteasome system (UPS) and activation of autophagy-related pathways (Sandri, 2013). For example, muscle-specific E3 ubiquitin ligases, such as muscle RING finger protein 1 (MURF1), are key enzymes that facilitate conjugation of ubiquitin to specific target proteins, leading to their degradation via the proteasome (Bodine et al., 2001; Cohen et al., 2012; Perera et al., 2011). In addition, activation of the autophagy system enhances the breakdown of long-lived proteins, protein aggregates, and organelles. During the highly orchestrated process of autophagy, the cargo is engulfed by autophagosomes, which then fuse to lysosomes, leading to degradation of the contents by proteases (Klionsky, 2005). This system is highly error-prone, and impairments of autophagy are implicated in a variety of diseases, including inherited muscle diseases, also referred to as autophagic vacuolar myopathies (AVMs), as well as multisystem proteinopathies (MSPs) (Nishino, 2003).

Denervation of the sciatic nerve provides a model to study enhanced protein breakdown in muscle in living mice (Furuno et al., 1990; Schiaffino and Hanzlíková, 1972). Loss of neuronal stimulation induces rapid loss of muscle mass and leads to reduced muscle performance. Although activation of the UPS is primarily responsible for the degradation of 80%–90% of all proteins (Rock et al., 1994), it is not entirely clear how the autophagy system interacts with the UPS and contributes to overall remodeling during catabolic conditions (Lilienbaum, 2013). Previous studies showed that not all muscles are equally affected by atrophy and respond very differently, depending on their fiber type composition (Ciciliot et al., 2013; Lang et al., 2017; Schiaffino and Reggiani, 2011).

In addition, a set of molecular chaperones is responsible for the correct assembly and degradation of macromolecular structures (Hartl et al., 2011). Molecular chaperones are important because the proteins of the contractile apparatus must be continuously replenished in post-mitotic muscle fibers. Notably, heat shock proteins, including the HSP70 family and α-crystallin, are more abundant in slow fibers compared with fast fibers,

reflecting higher protein turnover and enhanced oxidative capacity (Drexler et al., 2012; Goldberg, 1967).

Several recent studies showed that protein methyltransferases not only target histones but also modify a wide range of cytoplasmic proteins (Clarke, 2013). However, the functions and targets of most of the ~200 putative S-adenosyl methionine (SAM)-dependent methyltransferases (MTases) remain unknown. The majority of protein methyltransferases are class I MTases that consist of a twisted seven-stranded β sheet (7BS) with four conserved motifs (motif I, post I, motif II, and motif III), and a representative group is MTase family 16 (MTF16), whose members preferentially methylate molecular chaperones (Cloutier et al., 2013). CAM-KMT is an MTF16 family member that specifically trimethylates K115 of calmodulin, which alters the calmodulin interaction network (Magnani et al., 2010). Similarly, METTL21A (HSPA-KMT) methylates HSPA8 and, thereby, inhibits its interaction with the Parkinson disease-associated protein α-synuclein (Jakobsson et al., 2013). Another member of the MTF16 family, METTL21B, methylates eukaryotic initiation factor 1A (eEF1A) on K165; this modification has been suggested to regulate eEF1A activity in a tissue-specific manner (Malecki et al., 2017).

The most extensively studied MTF16 family member is METTL21D (VCP-KMT), which catalyzes the trimethylation of K315 on p97/VCP, a ubiquitously expressed chaperone containing two ATPase domains (Kernstock et al., 2012). p97 assembles into a homohexameric complex and is involved in various processes, including vesicle transport and disintegration of protein aggregates, as well as ubiquitin-proteasome-dependent and autophagosome-lysosome-dependent protein breakdown (Jentsch and Rumpf, 2007; Latterich et al., 1995; Meyer and Weihl, 2014). Mutations of the *p97* gene are causative for several rare multisystem degenerative disorders, including inclusion body myopathy associated with Paget disease of the bone and frontotemporal dementia (IBMPFD) and amyotrophic lateral sclerosis (ALS) (Custer et al., 2010; Kimonis et al., 2008). Muscle weakness is the first symptom in over 50% of p97-associated diseases (Ju et al., 2009). Other typical symptoms are accumulation of non-digested autophagosomes and poly-ubiquitin aggregates. Furthermore, regulation of p97 activity is highly dependent on its interactions with co-factors and post-translation modifications (Buchberger et al., 2015).

The role of another MTF16 family member, METTL21C, is poorly described. Earlier studies in HEK293 cells showed that METTL21C potentially interacts with HSP70 (Cloutier et al., 2013), and genome-wide association studies (GWAS) identified that METTL21C may function as a pleiotropic factor in muscle (Huang et al., 2014). However, the exact physiological function of this muscle-specific methyltransferase and its substrates are completely unknown.

In this study, we demonstrate that METTL21C protein expression is restricted to MYH7-positive muscle fibers. Genetic ablation of *Mettl21c* in the mouse resulted in reduced running capacity as well as decreased p97 trimethylation at position K315, which obstructed p97 hexamer assembly and reduced ATPase activity.

RESULTS

METTL21C Expression Is Restricted to Slow and Mixed Skeletal Muscle Fibers

A previous proteomic study of various mouse muscles demonstrated enhanced protein expression of METTL21C in the slow soleus compared with the fast *extensor digitorum longus* (EDL) muscle (Drexler et al., 2012). We quantified expression of *Mettl21c* in various mouse tissues, and detected the transcript exclusively in skeletal muscle tissue (Figure 1A). Comparison of METTL21C expression in different hindlimb muscles using a customized antibody revealed a positive correlation between METTL21C protein expression and the proportion of slow type I fibers (Figure 1B). The highest signal for METTL21C was identified in the *gluteus maximus* (GLUT), whereas, in the EDL, a fast muscle, very low levels of METTL21C were detected. Immunostaining of longitudinal human skeletal muscle cryosections revealed a highly regular striated pattern of endogenous METTL21C expression that co-localized with the Z-disk protein α-actinin-2 and did not overlap with the M-band marker protein myomesin-2 (Figure S1A).

To gain insight into the physiological function of METTL21C, we generated a knockout mouse strain via homologous recombination (Figure S1B). *Mettl21c* gene ablation was achieved by replacing the coding region from exon 2 to exon 5 with a β-galactosidase (lacZ) cassette; successful deletion was confirmed by PCR (Figure S1C), immunoblotting (Figure 1C), and mass spectrometry (MS) using an *in vivo* stable isotope labeling by amino acids in cell culture (SILAC) approach (Figure 1D). *Mettl21c*$^{-/-}$ mutants were born at normal Mendelian rates, were viable and fertile, and did not show any obvious morphological or physiological changes in the skeletal muscles (Figures S1D–S1I). Expression analysis of the lacZ reporter inserted into the *Mettl21c* gene locus using β-galactosidase staining showed that the signal was restricted to skeletal muscle tissue during the postnatal and adult stages (Figure S1J). Next we stained muscle cross-sections using lacZ and antibodies against the fiber type-specific fast myosin heavy chain 2 (MYH2) and slow MYH7 isoforms (Figures 1E and 1F; Figure S1K); METTL21C was primarily expressed in slow muscle fibers. Further, inactivation of METTL21C did not induce fiber type switching (Figure S1I), indicating that METTL21C is not involved in fiber type specification.

Next we performed single fiber proteomics analysis. MS analysis of 20 randomly selected muscle fibers from the soleus confirmed the ~1:1 composition of type I and type IIa fibers with a minor fraction of mixed fibers (Figure 1G). Next we conducted β-galactosidase staining of muscle fibers from *Mettl21c*$^{+/-}$ animals and found that all 20 selected blue lacZ-positive fibers were positive for the slow MYH7 isoform. A third of fibers were classified as mixed fibers, expressing both the MYH7 and MYH2 isoforms (Figure 1H). Although MYH7 is also expressed in heart tissue, we did not detect any expression of METTL21C in the heart, as indicated by qPCR analysis (Figure 1A) and absent β-galactosidase staining (data not shown). In conclusion, METTL21C is predominantly expressed in pure type I fibers but is also detectable in mixed MYH7 and MYH2 fibers.

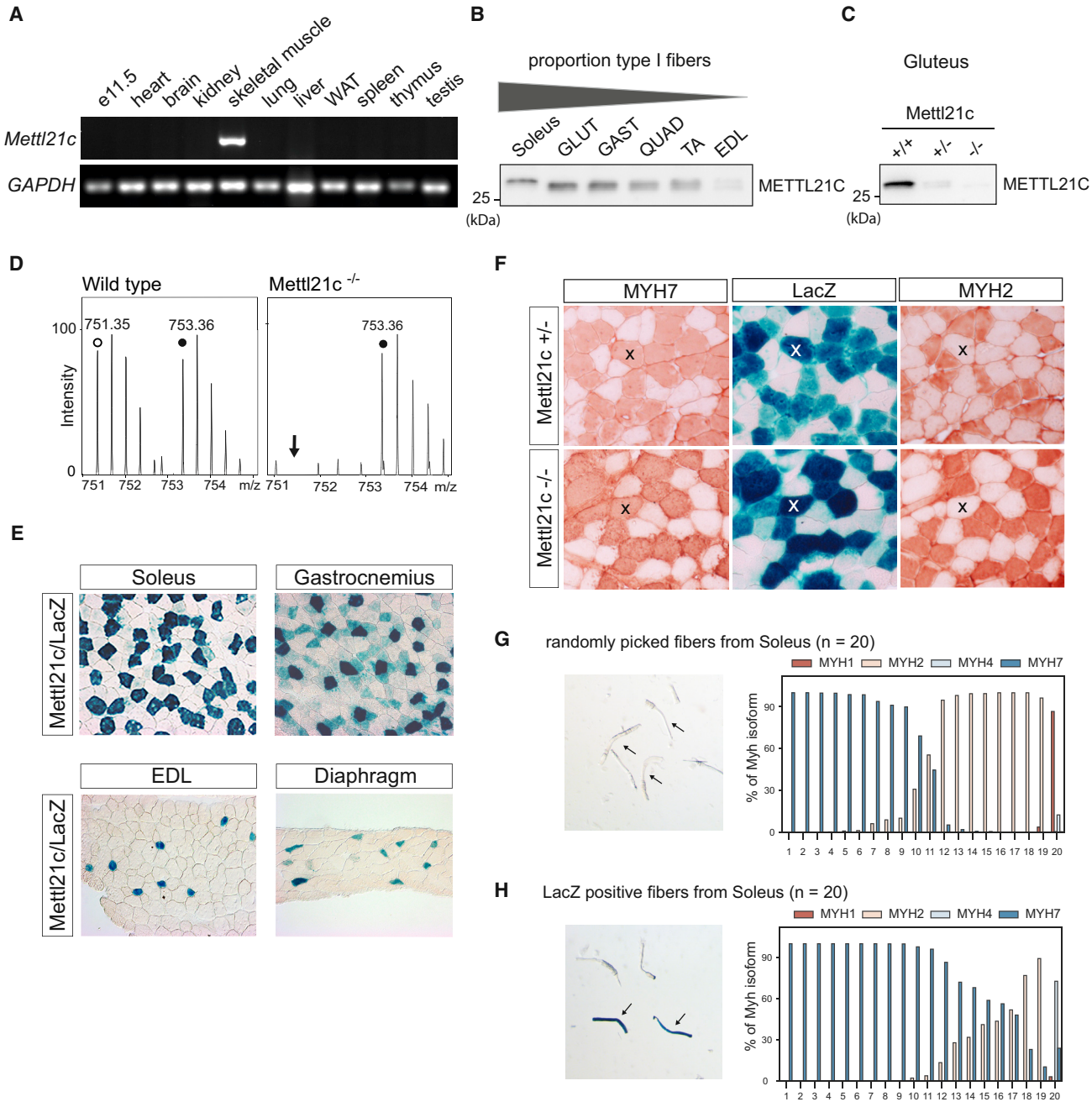

Figure 1. METTL21C Expression Is Restricted to MYH7-Positive Muscle Fibers

(A) *Mettl21c* mRNA expression analysis in mouse embryos (embryonic day 11.5 [E11.5]) and adult mouse tissues.

(B) Immunoblot of METTL21C in protein extracts from various skeletal muscles. Muscles are arranged according to slow type I fiber content.

(C) Immunoblot of METTL21C in gluteus lysates from mice with the indicated genotypes.

(D) Mass spectrometry analysis-derived SILAC spectra of the METTL21C peptide (METTL21C: ^{42}FVPTDYASYTQEHYQFAGK^{60}) at *m/z* 751.35 (charge 3+). The white circle represents the non-labeled METTL21C peptide, whereas the black circle indicates the corresponding heavy Lys6-labeled peptide. The arrow in the right MS spectrum marks the absence of the corresponding non-labeled peak at 751.35 *m/z* in the *Mettl21c*$^{-/-}$ mutant.

(E) β-Galactosidase staining of cryosections from *Mettl21c*$^{+/-}$ mutants showing lacZ-positive cells in the soleus, GAST, and, to a lesser extent, in the EDL and diaphragm.

(F) Immunohistochemical staining of consecutive sections from *Mettl21c* heterozygous and homozygous mutant soleus muscle using MYH7 antibody (left), β-galactosidase staining (center), and MYH2 antibody (right). Identical fibers in serial cryosections (20 μm) are labeled with X.

(G and H) Separated soleus fibers (arrows) were selected randomly (G), or only lacZ-positive fibers were selected after β-galactosidase staining (H), and single-fiber mass spectrometry was used to determine MYH isoform intensities. Each bar represents, for one fiber, the relative abundance of the MYH isoforms in relation to the total sum of MYH1, MYH2, MYH4, and MYH7 intensities.

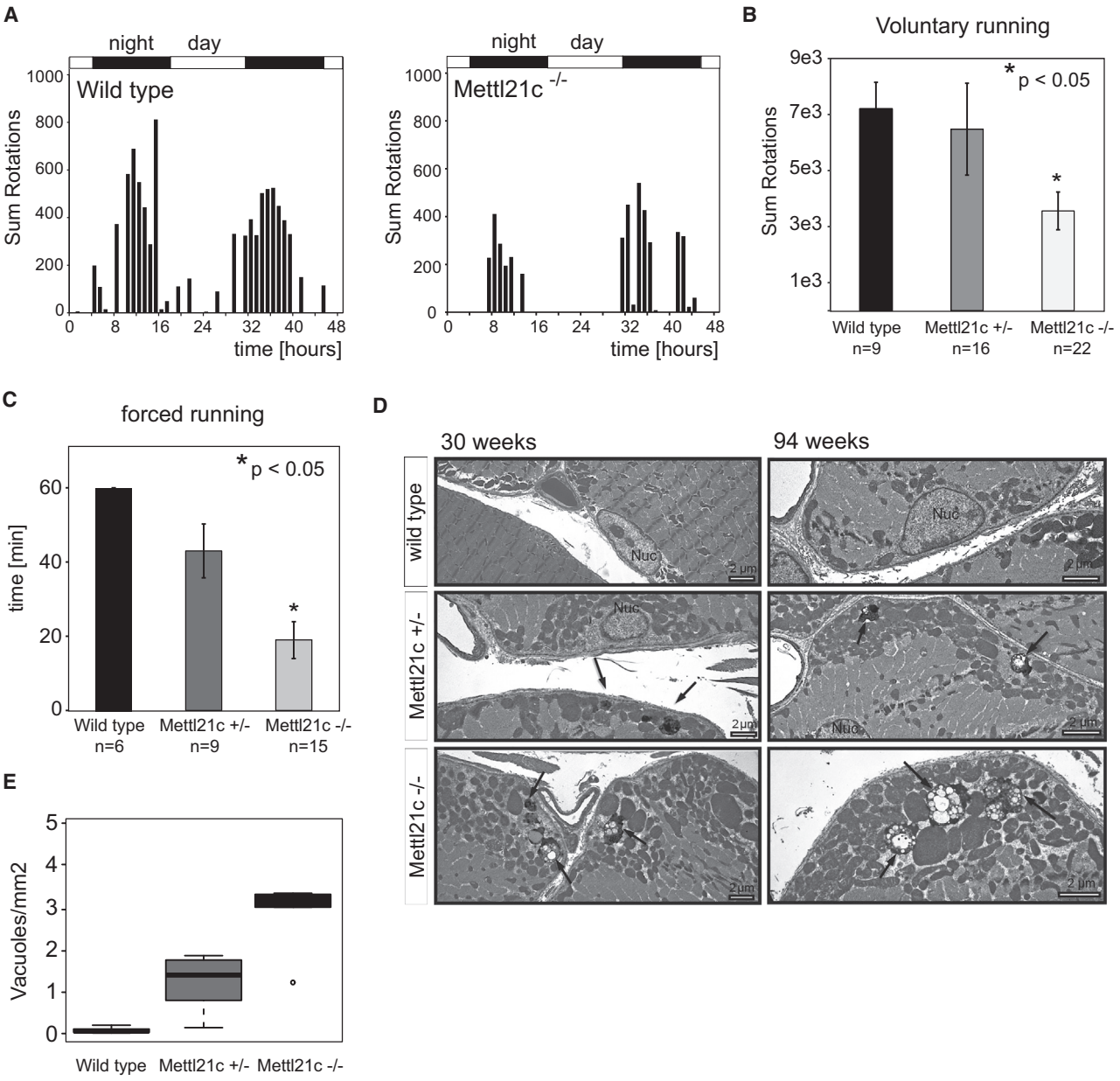

Figure 2. Genetic Ablation of *Mettl21c* in Mice Leads to Reduced Muscle Performance and Age-Dependent Accumulation of Vacuolar Structures in Skeletal Muscle

(A and B) Voluntary wheel running activity during the night and day for wild-type and *Mettl21c*$^{-/-}$ littermates over 2 consecutive days. The sum of rotations is shown per hour for one representative wild-type and mutant pair (A) as well as the average total values for the indicated numbers of mice per genotype (B).

(C) Treadmill exercise performance test. The average duration the animals were able to run at a velocity of 12 m/min is shown for the indicated numbers of mice per genotype. The p values were calculated using unpaired two-sided t tests. Bar plots indicate mean ± SD.

(D) Representative electron micrographs of the soleus of wild-type, *Mettl21c*$^{+/-}$, and *Mettl21c*$^{-/-}$ mice. Left: 30-week-old animals. Right: 94-week-old animals. Arrows indicate vacuolar structures. Scale bars, 2 µm.

(E) Boxplot analysis of the quantities of vacuoles based on electron micrograph analysis (n = 3).

Deletion of Mettl21c Reduces Running Performance and Leads to Accumulation of Autophagic Vacuoles

Running tests were chosen as a means of characterizing muscle performance in control and *Mettl21c*$^{-/-}$ mice. Voluntary running was assessed using the sum of wheel rotations per night; we observed a significant reduction of over 50% in *Mettl21c*$^{-/-}$ mutants compared with controls (Figures 2A and 2B). Forced running experiments were performed on a treadmill at a constant velocity of 12 m/min. Wild-type mice (n = 6) were able to run constantly for at least 1 hr, whereas

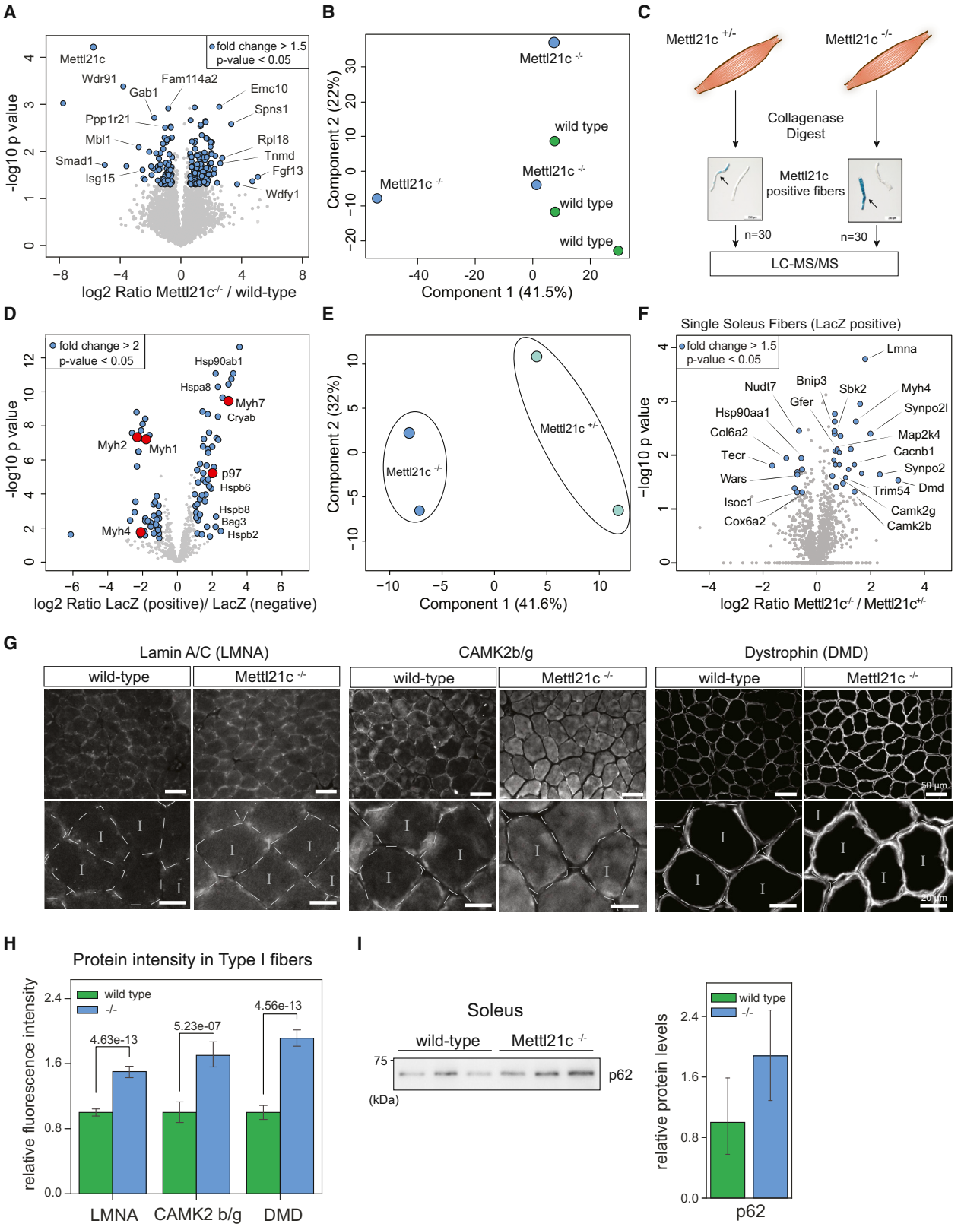

(legend on next page)

Mettl21c$^{-/-}$ animals were fatigued after an average of 20 min (Figure 2C).

Next we analyzed the ultrastructure of the soleus from 30- and 94-week-old mice by electron microscopy. We identified accumulation of residual structures in *Mettl21c*$^{-/-}$ mutants, likely the result of incomplete autophagy processes during aging (Figures 2D and 2E). These structures were similar in appearance to lipofuscin granules and autophagic vacuoles. In some cases, vesicular structures were found in direct proximity to mitochondria or protein aggregates (Figure S2A). These alterations might resemble the phenotypes observed in AVM and have often been associated with pathological neuromuscular disorders (Fukuhara et al., 1980).

Loss of METTL21C Dysregulates Proteins Involved in Proteostasis

Next we used an MS label-free protein quantification approach to compare the protein changes in the soleus of wild-type and *Mettl21c*$^{-/-}$ mutant mice and quantified 6,317 proteins (Table S1). Statistical analysis based on a two-sided t test revealed 121 upregulated and 74 downregulated proteins (Figure 3A). The Pearson correlation coefficients between all replicates were higher than 0.90, demonstrating robust protein quantification (Figure S3A). We identified that METTL21C was significantly downregulated ($\log_2$ *Mettl21c*$^{-/-}$/wild-type ratio = −5.77; $-\log_{10}$ p = 4.22). Next we performed principal-component analysis (PCA) and observed no clear clustering between the triplicate muscle samples from wild-type and *Mettl21c*$^{-/-}$ mutant mice (Figure 3B). Because METTL21C is predominantly expressed in slow fibers, it is possible that other fibers that do not express METTL21C compensate or cover the potential effect of *Mettl21c* gene inactivation in slow fibers.

To focus our analysis on slow fibers, we used collagenase digestion to disaggregate soleus fibers from *Mettl21c*$^{+/-}$ and *Mettl21c*$^{-/-}$ mutants. After incubation with lacZ staining solution for 1 hr, we pooled 30 blue fibers to perform a fiber type-specific proteomics analysis (Figure 3C). To validate this approach, we first compared lacZ-positive (blue) and -negative (white) fibers. Slow MYH7 was consistently highly expressed in blue fibers, whereas white fibers expressed the fast MYH isoforms (Figure 3D; Table S2), demonstrating the applicability of our approach. Moreover, slow fibers also revealed enhanced expression of several heat shock proteins and chaperones, including HSP90, HSPB2/6/8, and the ATPase p97.

Proteomics analysis of 30 blue fibers from *Mettl21c*$^{+/-}$ and *Mettl21c*$^{-/-}$ mutants revealed 1,564 quantified proteins with a Pearson correlation coefficient between biological replicates ranging from 0.97 to 0.98 (Figure S3B; Table S2). In contrast to the previous PCA based on the intact soleus, clear separation was observed between the control (*Mettl21c*$^{+/-}$) and the *Mettl21c*$^{-/-}$ group (Figure 3E). The analysis identified 37 significantly regulated proteins (Figure 3F). Among the proteins upregulated in *Mettl21c*$^{+/-}$ slow fibers, we found candidates involved in skeletal muscle architecture and contraction, including dystrophin (DMD), synaptopodin-2 (SYNPO2), and the Ca^{2+}/calmodulin-dependent protein kinase II subunits β/γ (CaMK2b/g). Lamin A/C (LMNA), a nuclear envelope protein required for muscle satellite cell differentiation and myonucleus stability (Frock et al., 2006), was also upregulated. In addition, several proteins implicated in proteostasis were dysregulated: the ubiquitin E3 ligase TRIM54 (also named MURF3), the heat shock protein HSP90AA1, and BNIP3, which mediates the degradation of mitochondrial proteins (Shi et al., 2014). We confirmed the dysregulation of several proteins via immunostaining of muscle cross-sections of wild-type and *Mettl21c*$^{-/-}$ soleus (Figures 3G and 3H; Figure S3C). Co-staining with a MYH7 antibody was used to identify slow muscle fibers (Figure S3D). In addition, immunostaining and immunoblotting revealed that LC3 and p62, markers of autophagy, were both upregulated in *Mettl21c*$^{-/-}$ mutants (Figure 3I; Figure S3C). Overall, these results show that loss of METTL21C primarily affects slow fibers and provokes differential regulation of various proteins associated with protein breakdown.

METTL21C Modulates Autophagic Flux during Denervation-Induced Atrophy

To investigate whether METTL21C is directly involved in protein breakdown, we performed dissection of the sciatic nerve in mice to induce muscle atrophy (Figure S4A). We observed an equal muscle weight reduction of ∼35% in the denervated leg of both wild-type and *Mettl21c*$^{-/-}$ mutant mice compared with the non-denervated control leg 7 days after denervation

Figure 3. Fiber Type-Specific Proteomic Profiling of *Mettl21c*$^{-/-}$ Mutants Reveals Dysregulation of Proteostasis-Related Proteins

(A) Differentially regulated proteins in the intact soleus muscle of wild-type and *Mettl21c*$^{-/-}$ mutants (n = 3). Significantly regulated proteins are marked in blue (absolute [abs.] $\log_2$ fold change > 0.58, $-\log_{10}$ p > 1.3).

(B) Principal component analysis (PCA) 2D plot. Each dot represents one replicate from wild-type (green) or *Mettl21c*$^{-/-}$ mutant (blue) mice; n = 3.

(C) Experimental workflow for separation of β-galactosidase-positive slow-twitch fibers isolated from the soleus of *Mettl21c*$^{+/-}$ and *Mettl21c*$^{-/-}$ mice. The arrows indicate β-galactosidase-positive fibers.

(D) Volcano plot comparing protein fold changes between β-galactosidase-positive (blue) fibers (n = 57) and -negative (white) soleus fibers (n = 47). Significantly regulated proteins are labeled in blue (abs. $\log_2$ fold change > 1, $-\log_{10}$ p > 1.3). Red circles indicate MYH isoforms and p97.

(E) PCA 2 component plot. Replicates from *Mettl21c*$^{+/-}$ and *Mettl21c*$^{-/-}$ (n = 2) are encircled.

(F) Volcano plot of *Mettl21c*$^{-/-}$/*Mettl21c*$^{+/-}$ protein ratios (n = 2). Significantly altered proteins (abs. $\log_2$ fold change > 0.58 and $-\log_{10}$, p > 1.3) are marked in blue.

(G) Immunohistochemical staining for the indicated proteins in soleus cryosections from wild-type and *Mettl21c*$^{-/-}$ mice. Slow type I fibers were determined by co-staining with a MYH7 antibody.

(H) Quantification of average fluorescent signal intensities in MYH7-positive fibers for the immunostaining shown in (G). Fibers were selected and quantified using ImageJ (n = 13–19). Bar plots are relative mean ± 95% confidence interval (CI). The p values were calculated using unpaired two-sided t test.

(I) Immunoblots of p62 expression in soleus protein extracts from wild-type and *Mettl21c*$^{-/-}$ mutants. For quantification, protein levels were normalized to the stain-free loading control; bar plots are relative mean ± 0.95 CI (n = 3).

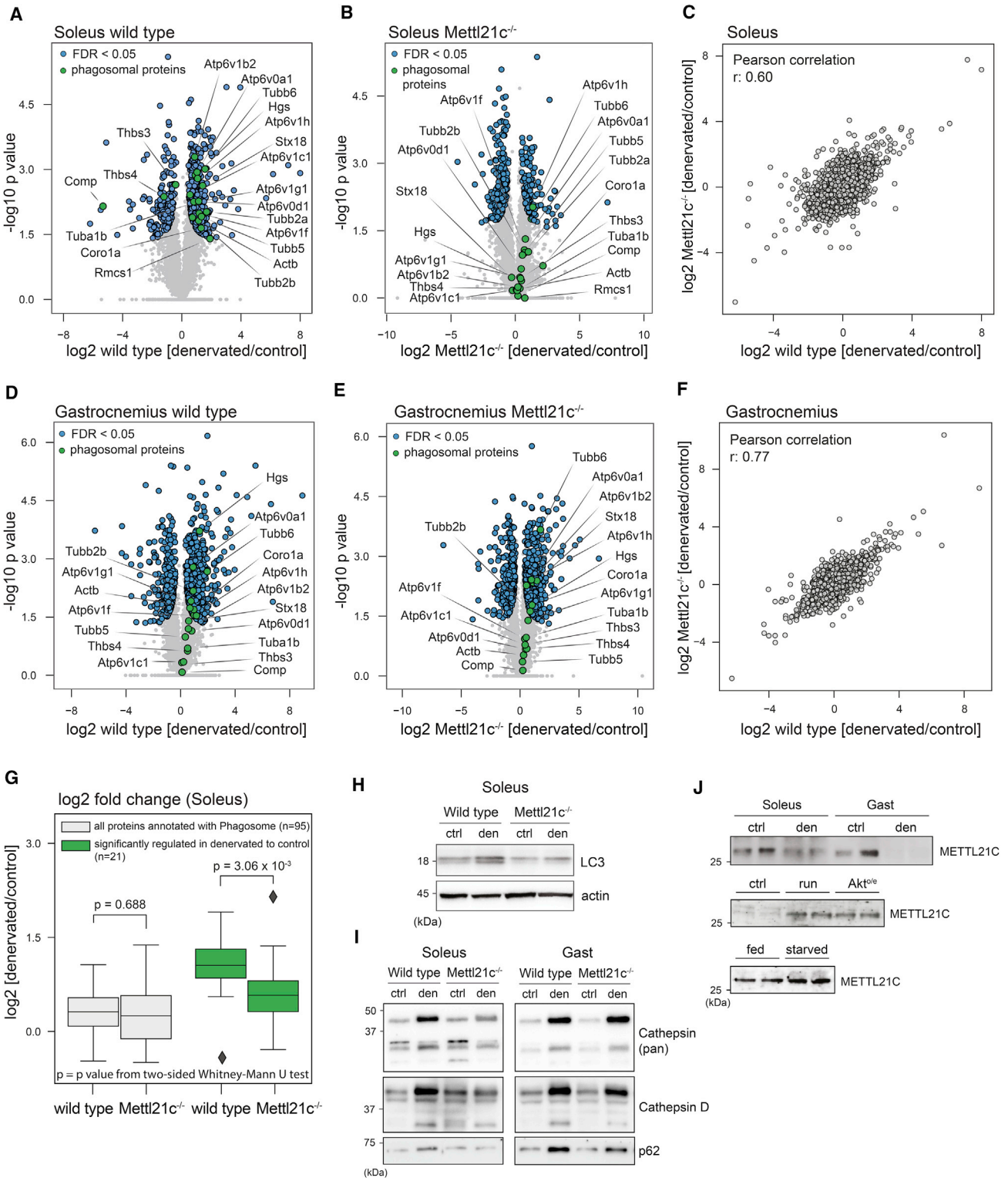

Figure 4. Inactivation of *Mettl21c* Negatively Affects Protein Degradation Pathways during Denervation-Induced Atrophy.

(A and B) Volcano plots comparing protein fold changes between soleus muscles from denervated and control legs in (A) wild-type and (B) *Mettl21c*$^{-/-}$ mice (n = 3). Blue circles represent significantly differentially regulated proteins (permutation-based FDR cutoff of 0.05). Several phagosomal proteins are indicated with green circles.

(C) Scatterplot of $\log_2$ control/denervated protein ratios from wild-type and *Mettl21c*$^{-/-}$ mice.

(legend continued on next page)

(Figure S4B). To assess the influence of METTL21C during muscle atrophy, we performed protein profiling of the soleus and gastrocnemius (GAST) from wild-type and *Mettl21c*$^{-/-}$ mutant mice (Figures 4A, 4B, 4D, and 4E; Table S3). Of note, we found, under all conditions, more proteins significantly upregulated than significantly downregulated, except for the soleus of *Mettl21c*$^{-/-}$ mice, where 124 proteins were upregulated and 195 were downregulated (Figure S4C).

Next we assigned gene ontology (GO) annotations and performed Fisher's exact test to identify enriched GO terms in the group of significantly regulated proteins using a 5% false discovery rate (FDR) cut-off (Benjamini-Hochberg correction) (Figures S4D–S4G). Although we found that GO terms associated with protein breakdown, such as phagosome, proteasome, and positive regulation of catabolic processes, were enriched after denervation in control mice, these terms were not identified for *Mettl21c*$^{-/-}$ mice. The GO term phagosome includes several vacuolar ATPase subunits (ATP6V0A1, ATP6V1B2, etc.) that were significantly altered in the soleus of wild-type animals after denervation. This response was abolished in *Mettl21c*$^{-/-}$ animals, as highlighted in the volcano plots by indication of phagosomal proteins by green circles (Figures 4A, 4B, 4C, and 4D). This discrepancy only applied to a specific subset of 21 phagosomal proteins ($p = 3.06e{-3}$); comparison of all phagosomal proteins ($n = 95$) revealed no significant difference ($p = 0.688$) between genotypes (Figure 4G). In addition, a difference in phagosomal proteins was not observed between the GAST of wild-type and *Mettl21c*$^{-/-}$ mice. Accordingly, the Pearson correlation (r) for all protein ratios between wild-type and *Mettl21c*$^{-/-}$ mice was 0.60 in the soleus compared with the higher correlation of 0.77 for the GAST (Figures 4C and 4F). This result suggests that the soleus is more affected by the loss of METTL21C than the GAST during muscle atrophy.

To evaluate whether ablation of *Mettl21c* leads to dysregulation of other proteins related to protein degradation, we performed immunoblotting for LC3 to monitor the formation of autophagosomes. We found enhanced levels of LC3 and its lipidated form in denervated wild-type soleus, reflecting induction of autophagy. Conversely, we identified virtually no LC3 lipidation in the soleus of *Mettl21c*$^{-/-}$ mice after denervation (Figure 4H). In addition, we examined the changes in cathepsins, lysosomal proteases involved in autophagosomal protein breakdown. Immunoblotting using a pan-cathepsin and cathepsin D antibody revealed reduced induction of the precursor and processed forms after denervation in *Mettl21c*$^{-/-}$ mutants (Figure 4I). p62, an autophagosomal transport protein, was not upregulated after denervation in *Mettl21c*$^{-/-}$ mutants compared with wild-type animals. Notably, these effects again seemed more pronounced in the soleus.

As evidenced by our quantitative MS analysis and immunoblotting, METTL21C expression was largely abolished in the GAST 7 days after denervation (Figure 4J; Table S3), whereas we observed no change in METTL21C in the soleus 7 days after denervation. Next we performed treadmill exercise tests for 2 hr and observed increased METTL21C protein expression in the soleus (Figure 4J). Similarly, using inducible muscle-specific AKT overexpression as a model of hypertrophy (Blaauw et al., 2009) or starving animals for 24 hr both increased the levels of METTL21C.

In conclusion, METTL21C is required under conditions of enhanced protein breakdown, and its inactivation results in impaired induction of proteins involved in the autophagy-lysosome pathway.

METTL21C Interacts with Chaperones and Induces Trimethylation of p97 at K315, Affecting Hexamer Assembly

To identify potential interactors of METTL21C, we performed SILAC-based liquid chromatography-tandem MS (LC-MS/MS) immunoprecipitation (IP) experiments after expressing GFP-tagged METTL21C in HEK cells (Figure S5A; Table S4). We identified interaction with several chaperones, including BAG2, BAG6, HSPB1, p62, and p97, although these factors were not detected under all experimental conditions. The interaction with p97 was further confirmed through endogenous co-immunoprecipitation (coIP) with METTL21C from gastrocnemius lysates (Figure 5A). The ATPase p97 plays an important role in protein degradation in skeletal muscle and is upregulated in response to denervation-induced atrophy (Piccirillo and Goldberg, 2012). We assessed the levels of p97 in the soleus and GAST 7 days after denervation and observed more pronounced upregulation of p97 in the GAST compared with the soleus (Figure 5B). Relating this to our earlier observation of dynamic changes in METTL21C levels (Figure 4J), this suggests that METTL21C could be directly involved in the regulation of p97 protein abundance during early muscle atrophy.

Because of its similarity with METTL21D and the physical interaction between METTL21C and p97, we hypothesized that METTL21C methylates p97. To prove this, we performed an *in vitro* methyltransferase assay (Figure 5C). As a negative control, we used a catalytically inactive METTL21C variant containing three mutated glycine residues in the consensus protein sequence (at positions 101–108 [LEIGAGAG] to alanine [LEIAAAAA]), which results in impaired SAM binding (Kozbial and Mushegian, 2005). To identify methylation sites, we combined our *in vitro* assay with MS. Several methylation sites were detected after incubation with METTL21C, including 10 mono-, 6 di-, and 1 trimethylation site on p97 (Figure 5D;

(D and E) Volcano plots for the GAST muscle from wild-type (D) and *Mettl21c*$^{-/-}$ mice (E), as in (A) and (B) ($n = 3$).
(F) Scatterplot for the GAST muscle as in (C).
(G) Boxplot analysis illustrating the fold changes for all phagosomal proteins ($n = 95$; left) and a subset of significantly regulated phagosomal proteins ($n = 21$; right) in the soleus of wild-type and *Mettl21c*$^{-/-}$ mice. The p values were calculated using the Whitney-Mann *U* test.
(H) Immunoblot of LC3 in denervated (den) and control (ctrl) soleus protein extracts from mice with the indicated genotypes.
(I) Immunoblots of pan-cathepsin, cathepsin D, and p62 expression.
(J) Immunoblot of METTL21C expression in muscle lysates after various stress conditions: den, 7 days after denervation of sciatic nerve; run, 2 hr running until exhaustion; Akt$^{o/e}$, induced Akt overexpression in skeletal muscle (hypertrophy model); starved, starvation for 24 hr.

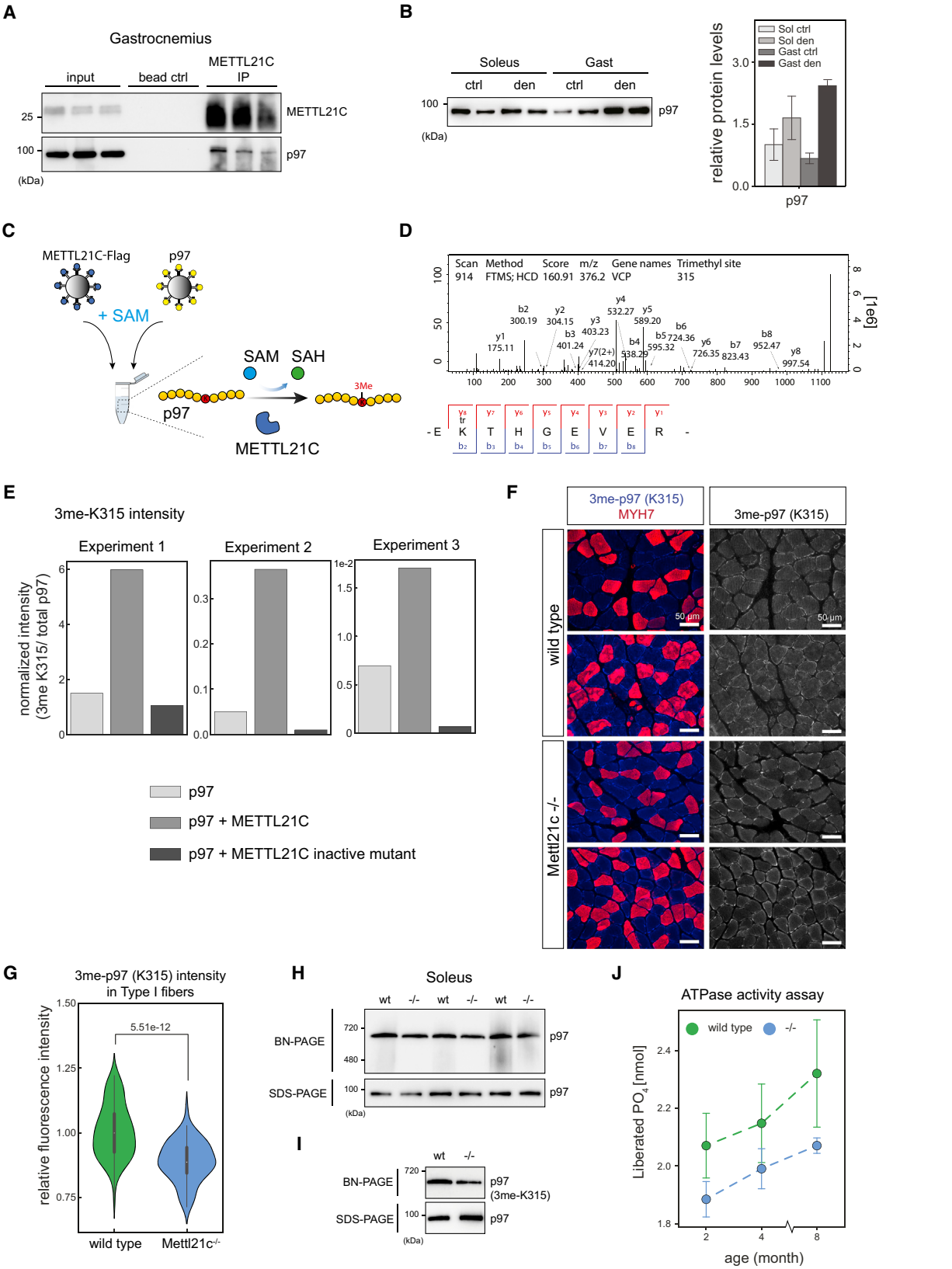

(legend on next page)

Figure S5B; Table S5). However, only the p97 K315 trimethylation site showed enhanced intensity after incubation with METTL21C; the other p97 methylation sites were detected at equal intensities under all experimental conditions (Figure 5E; Table S5). The same experiment was performed with recombinant proteins (Figure S5C; Supplemental Experimental Procedures), but we could not reproduce the methylation activity. We suppose that missing post-translational modifications, such as mono- and di-methylation of METTL21C (Table S5), and/or lack of further co-factors are the reason for that.

Further support that METTL21C trimethylates p97 *in vivo* was obtained by immunostaining of soleus cross-sections with an antibody that specifically recognizes K315 trimethylation of p97, showing reduced signal intensity in the slow fibers of *Mettl21c*$^{-/-}$ animals (Figures 5F and 5G).

To assess whether reduced trimethylation influences p97 complex formation, we performed a blue native PAGE (BN-PAGE), which revealed that reduced p97 hexamer assembly occurred in parallel to reduced K315 trimethylation (Figures 5H and 5I). Next, we used gel filtration to fractionate HEK cell lysates after overexpression of METTL21C-FLAG. Because the main peak intensities of the p97 hexamer eluted in fractions with higher molecular weight compared with the METTL21C-FLAG construct, we suggest that METTL21C interacts with and methylates p97 monomers (Figure S5D). This could possibly explain the weak interaction between METTL21C and p97 because the majority of p97 is present in assembled hexamer. Next, we assessed p97 ATPase activity and observed reduced ATPase activity in *Mettl21c*$^{-/-}$ mutants of different ages compared with controls (Figure 5J).

Using site-directed mutagenesis, we substituted lysine 315 with alanine to generate a methylation-deficient p97 mutant (K315A). p97 wild-type and p97 K315A FLAG fusion constructs were then overexpressed in HEK cells and used for BN-PAGE analysis and ATPase activity assays. We observed no obvious change in hexamer formation (Figure S5E) but a significant reduction in ATPase activity for the K315A mutant (Figure S5F). Because we used total cell lysates for the BN-PAGE experiments, it is possible that endogenous p97 will continue to be methylated and form hexamers. We presume that this obliterates the effects of the methylation-deficient mutant.

Accumulation of UNC45B, a well-characterized substrate of p97, in *Mettl21c*$^{-/-}$ slow fibers supports the hypothesis that p97 activity was decreased (Figure S5G). Overall, this evidence strongly suggests that the slow muscle-specific lysine methyltransferase METTL21C trimethylates p97 at position K315, modulating p97 hexamer formation and activity in skeletal muscles.

DISCUSSION

Mettl21c Inactivation Leads to Dysregulation of Proteins Linked to Proteostasis in Slow Muscle Fibers

Our fiber type-selective proteomics analysis of wild-type and *Mettl21c*$^{-/-}$ mutant muscles revealed dysregulated expression of proteins involved in several aspects of proteostasis, including protein folding (HSP90AA1), protein degradation (TRIM54), and autophagy (SYNPO2). We were only able to detect these changes in slow muscle fibers, which clearly demonstrates a heterogeneous response of different muscle fibers. Furthermore, these results highlight the potential of fiber type-specific proteomics as a very promising approach to study the response of individual fibers with distinct metabolic profiles and MYH contents in response to perturbations.

Although we only observed moderate changes for selected proteins in the quantitative proteomic analysis, it is likely that minor variations in protein turnover within skeletal muscle could induce profound effects over time and might reflect the progression of human muscle diseases during aging. Muscle fibers rely on tight regulation of protein degradation, which is crucially important to deplete the damaged proteins that arise from force generation-dependent mechanical and oxidative stress in muscle tissue. A reduced ability to remove damaged or misfolded proteins inevitably interferes with muscle performance.

In *Mettl21c*$^{-/-}$ mutants, we found increased levels of BNIP3, which functions as an autophagy receptor for mitochondrial proteins (Hanna et al., 2012); this finding suggests interference with mitochondrial activity. Our proteomics analysis did not identify any significant changes in mitochondrial proteins, including proteins responsible for fusion and fission, in *Mettl21c*$^{-/-}$ mutants. However, we cannot entirely exclude the possibility of impaired mitochondrial activity. Analysis of mitochondrial DNA mutation

Figure 5. METTL21C Is Responsible for p97 K315 Trimethylation in Skeletal Muscle and Modulates p97 Hexamer Formation and ATPase Activity

(A) Immunoblot of METTL21C and p97 from GAST lysates showing levels before (input) and after METTL21C immunoprecipitation (IP). Protein A beads without antibody were incubated with lysates to determine background binding (bead ctrl).

(B) Immunoblot of p97 in den and ctrl muscles. For quantification, protein levels were normalized to the stain-free loading control, and the bar plots represent the relative mean ± 0.95 CI (n = 2).

(C) Experimental setup of the *in vitro* methylation assay.

(D) Selected MS/MS scan of the p97 peptide with trimethylated K315 and annotated *b*- and *y*-ions.

(E) *In vitro* methylation assay. Bar plots display the normalized intensity of the trimethylated K315 peptide with respect to the control reaction in three independent experiments.

(F) Immunostaining of soleus cryosections with an antibody specific for trimethylated K315. Slow type I fibers were identified by co-staining with MYH7 antibody.

(G) Violin plots showing the distribution of trimethylated (3me)-p97 (K315) fluorescence intensity in type I fibers. Intensity was calculated using ImageJ (n = 80, 40 fibers from 2 animals/genotype). The p value was calculated using Whitney-Mann *U* test.

(H) The abundance of p97 hexamers in soleus protein extracts was analyzed under non-denaturing conditions by blue native PAGE (BN-PAGE). An equal amount of each sample was separated by SDS-PAGE; total p97 levels were determined by immunoblotting and served as a loading control.

(I) BN-PAGE and SDS-PAGE as in (F), followed by immunoblotting for trimethylated K315 and p97.

(J) ATPase activity assay. p97 was immunoprecipitated from soleus lysates from 2-, 4-, and 8-month-old mice. Dots represent mean ± 0.95 CI for two technical replicates.

accumulation, mitophagy, and oxidative stress may help to elucidate whether METTL21C also affects muscle performance by regulating mitochondrial activity.

METTL21C Is Involved in Protein Remodeling during Denervation-Induced Muscle Atrophy

The ubiquitin-like modifier LC3/ATG8, an important marker protein of autophagy-related protein degradation, becomes anchored in the autophagosomal membrane and recruits important co-factors and cargo (Perera et al., 2011). Because we identified that neither form of LC3 was induced in *Mettl21c*$^{-/-}$ mutants after denervation, we suggest that autophagosome formation is impaired (Figure 4H).

The activity of several v-ATPases is required to generate a low pH within lysosomes, and fusion of acidic lysosomes with autophagosomes induces protein degradation (Sandri, 2013). The importance of these organelles was also emphasized by inactivation of *Lamp2* in the mouse, which inhibited formation of mature autophagosomes, led to improper cathepsin D processing, and increased p62 and LC3 levels (Nascimbeni et al., 2017; Tanaka et al., 2000). However, because we only examined the steady-state levels, it is not entirely clear whether the changes observed in *Mettl21c*$^{-/-}$ mutants reflect impaired induction of autophagy, reduced flux, or increased protein turnover. Detailed time-dependent assays after induction of atrophy in denervated or starved muscles combined with colchicine treatment are necessary to pinpoint which component(s) of the autophagy process is/are disturbed in *Mettl21c*$^{-/-}$ mutants.

We also found that METTL21C protein expression was rapidly downregulated in the wild-type GAST after denervation, whereas the soleus showed enhanced levels of METTL21C (Figure 4J). We therefore hypothesize that METTL21C may potentially determine the distinct responses of slow and fast fibers during atrophy demonstrated in earlier studies (Ciciliot et al., 2013). The elevated levels of METTL21C during various circumstances of increased protein remodeling (acute exercise, hypertrophy, and starvation) suggest a general function of METTL21C as a fiber type-specific regulator of protein turnover. Further mRNA expression analysis of *Mettl21c* during catabolic conditions is necessary to clarify the exact physiological function of METTL21C during stress-related conditions.

Trimethylation of p97 by METTL21C Is Required for p97 Hexamer Formation and Activity

We demonstrated that loss of p97 K315 trimethylation in *Mettl21c*$^{-/-}$ mutants led to reduced p97 hexamer formation and decreased ATPase activity in muscle. Because we used a full-length p97 construct, we were not able to determine whether this change in activity arises from the D1 or the D2 ATPase domain. However, we suggest that reduced p97 activity is an indirect effect resulting from impaired hexamer formation.

The family member METTL21D (VCP-KMT) is also capable of trimethylating p97 at position K315 (Cloutier et al., 2013), and previous studies found, in contrast to our observations, that this modification does not affect or even reduce p97 ATPase activity (Fusser et al., 2015; Kernstock et al., 2012). The opposing findings could have various reasons, one of them being the use of a recombinant p97 fragment, whereas we used endogenous full-length p97 immunoprecipitated from soleus lysates. We propose that our approach is more likely to represent the physiological situation. The differences between studies could also be related to other tissue-specific post-translational modifications (PTMs) or binding of co-factors, which will be investigated in future studies. However, we detected increased levels of UNC45B, a known substrate of p97 (Janiesch et al., 2007), which provides further evidence of reduced p97 activity in the skeletal muscle of *Mettl21c*$^{-/-}$ mutants.

Because protein methylation is essential for precise positioning of proteins within complexes and protein-protein interactions (Clarke, 2013; Erce et al., 2012), we propose that trimethylation of p97 is a common mechanism to regulate complex assembly and that tissue-specific methyltransferases are responsible for this modification. Although METTL21D is highly expressed in proliferative tissues (Fusser et al., 2015), METTL21C is limited to mature skeletal muscle; accordingly, only depletion of METTL21C seemed to affect the endurance of the mice in running experiments. We did not observe a complete loss of trimethylation in the slow muscle fibers of *Mettl21c*$^{-/-}$ mutants, which indicates the presence of genetic redundancy, possibly with compensation provided by other family members such as METTL21E or METTL22. Hence, it will be interesting to investigate the cross-talk within this modification network and examine how it influences p97 assembly, co-factor binding, and activity in both healthy muscle and disease-related conditions.

A Potential Role for METTL21C in Human IBMPFD

Next we discuss how these findings correlate to human patients with muscle weakness. Although the proportion of slow muscle fibers is considered relatively low in mice, we observed several phenotypic changes in *Mettl21c*$^{-/-}$ mutants, including muscle weakness, accumulation of vacuolar structures during aging, and dysregulation of several autophagy-related marker proteins, all symptoms of human muscle disorders. Humans have a much higher proportion of slow fibers than mice, suggesting that changes in METTL21C levels would have an even more pronounced effect in humans. Our finding that METTL21C regulates p97 activity is very important in this context because mutations in p97 that affect its activity have been linked to several rare MSPs in humans (Meyer and Weihl, 2014). For example, most of the p97 mutations detected in human patients with IBMPFD are localized at the N terminus within the first ATPase domain and enhance the ATPase activity of the D2 domain (Niwa et al., 2012). These p97 mutations impair autophagosome maturation, leading to accumulation of protein aggregates and muscle weakness (Tresse et al., 2010; Ju et al., 2009), which we also observed in our *Mettl21c* knockout mouse model.

We screened the genetic profiles of the cohort of patients with IBMPFD described by Nalbandian et al. (2012) and observed comparably low expression of *METTL21C* in two patients with either very late onset of symptoms or no symptoms. This indicates that reduced METTL21C protein expression could potentially exert a protective effect by lowering p97 activity, which may prevent the detrimental effects of hyperactive p97 mutant variants. Of course, this hypothesis requires intensive testing of larger cohorts of patients before any conclusions can be drawn.

Taken together, although deletion of *Mettl21c* in the mouse had no severe effects on muscle morphology under regular conditions, we believe that even small changes in p97 activity during aging provoke the accumulation of residues from incomplete autophagy processes, which leads to muscle weakness. Overall, this study demonstrates that METTL21C-dependent protein methylation influences the autophagy pathway in skeletal muscle, and we confidently conclude that this protein methylation is an important signal that modulates cellular plasticity in response to stress and aging in a tissue-specific manner.

EXPERIMENTAL PROCEDURES

Plasmids

The *Mettl21c* and *p97* coding sequences were amplified from mouse cDNA and inserted into the pCDNA5/TO vector (Invitrogen) in-frame with the FLAG epitope tag for overexpression in mammalian cells. Site-directed mutagenesis was used to mutate the three conserved glycine residues in motif I to alanine (*Mettl21c* GGG mutant) and lysine 315 to alanine (*p97* K315A mutant).

Expression Analysis

RNA was extracted from different tissues using TRIzol reagent (Invitrogen) based on the manufacturer's instructions. RNA was then reverse-transcribed into cDNA by RevertAid reverse transcriptase (Thermo Fisher Scientific). The PCR was performed using the following primer sequences for detection of the Mettl21c transcript: CAGGGGCTACAGCTCTGTGTC (forward) and CCCCCATACCAGTTCTCTCA (reverse).

Sciatic Nerve Transection

Mettl21c$^{-/-}$ mice and littermate control males (aged 8–12 weeks) were anaesthetized and denervated by removing ~5 mm of sciatic nerve from the left hindlimb. The right hindlimb served as the control leg. Wounds were closed by suturing with 5-0 Vicryl, and the site was checked daily for infection. After 7 days, the animals were euthanized by cervical dislocation, and the skeletal muscles were dissected and snap-frozen in liquid nitrogen. All mouse experiments were performed in accordance with institutional guidelines.

Voluntary and Forced Running Tests

For the voluntary running exercise, 2- to 3-month-old mice were given access to a cage equipped with a running wheel. After 1 day of acclimation, running performance was recorded using PhenoMaster software (TSE Systems) for 3 days. The forced running exercise was performed on a treadmill (Columbus Instruments) that provides a low-intensity electric shock to the paws of the mouse when the mouse stops running. Detailed experimental procedures are provided in the Supplemental Experimental Procedures.

Protein Extraction

Skeletal muscles were dissected and flash-frozen in liquid nitrogen. Frozen tissue was cryogenically ground using a mortar and pestle and resuspended in ice-cold lysis buffer (modified radioimmunoprecipitation assay [RIPA]: 50 mM Tris/HCl [pH 7.5], 150 mM NaCl, 1% NP-40, 1 mM EDTA, and 0.1% sodium deoxycholate) with protease inhibitor cocktail. After homogenization on a rotating wheel at 4°C for 30 min and sonication, crude extracts were clarified by centrifugation at 15,000 rpm at 4°C for 10 min. Cells were manually scraped and lysed using the same protocol.

Myofiber Isolation

Muscles from 8- to 12-week-old *Mettl21c*$^{-/-}$ mutants and littermate controls were carefully isolated and placed in collagenase solution (0.2% collagenase P in DMEM) and incubated at 37°C; the incubation time was adjusted depending on size, age, and muscle condition. The muscle was checked regularly to avoid over-digestion; digestion was stopped by transferring the muscle into pre-warmed DMEM, and then the muscle was gently flushed using a large glass pipette to release myofibers. The fibers were washed with PBS three times and collected under a stereo microscope (Leica).

β-Galactosidase Staining

After fixation in X-Gal fixation solution (100 mM sodium phosphate [pH 7.4], 0.2% glutaraldehyde, 2 mM $MgCl_2$, and 5 mM EGTA) for 5 min, samples were washed several times with X-Gal washing solution (100 mM sodium phosphate [pH 7.4], 0.02% NP40, 2 mM $MgCl_2$, and 0.01% Na-deoxycholate) and then incubated in X-Gal staining solution (X-Gal washing solution with 0.5 M K_3FeCN_6, 0.5 M K_4FeCN_6, and 0.1% X-Gal). The duration of incubation was adjusted depending on the sample (overnight for whole muscles, 1–12 hr for cryosections, and 1 hr for single myofibers). Washes were repeated three times, and samples were then prepared for imaging or other assays.

Cell Culture

HEK293T cells and C2C12 cells were cultured in DMEM high-glucose medium (Gibco) supplemented with 10% fetal bovine serum (FBS) and 1% penicillin-streptomycin-*L*-glutamine (PSG). Standard calcium phosphate transfection procedures were used to introduce the expression vectors into the cells. SILAC labeling of cells was performed as described previously (Krüger et al., 2008).

Immunoblotting

Equal amounts of protein lysates were separated using the tris-glycine extended (TGX) stain-free SDS-PAGE Mini-Protean system (Bio-Rad). Proteins were transferred onto polyvinylidene fluoride (PVDF) membranes using the Bio-Rad Trans-Blot Turbo system, and stain-free loading control images were acquired using the ChemiDoc imaging system (Bio-Rad). Proteins were detected using the following commercial antibodies: p62 (Abcam, ab91526), p97 (Abcam, ab11433), pan cathepsin (Santa Cruz Biotechnology, sc-6499), cathepsin D (Santa Cruz Biotechnology, sc-6486), LC3 (Cell Signaling Technology, 2775), pan actin (CST, 4968), FLAG M2 peroxidase (Sigma, A8592), methyl-p97 (Lys315, Merck, ABT286), and a custom-made METTL21C antibody (Abcore). After incubation with the corresponding secondary antibodies (Sigma), proteins were visualized by chemiluminescence using enhanced chemiluminescence (ECL) reagent (Bio-Rad) and imaged with the ChemiDoc imaging system (Bio-Rad).

Immunoprecipitation

Protein lysates (0.5–1 mg) from cells or skeletal muscle tissues were prepared as described previously and pre-cleared by incubation with Sepharose G beads for 30 min. Beads with non-specifically bound proteins were removed by centrifugation, the supernatant was incubated with 5–10 μg antibody for 30 min at 4°C, 30 μL Sepharose G beads were added, and incubation continued overnight. Alternatively, epitope tag beads were added directly after the pre-clearing step. On the following day, beads were washed four times with RIPA buffer. Proteins were eluted by heating the beads in 1.5× Laemmli buffer containing 40 mM DTT for 10 min at 70°C.

ATPase Activity Assay

p97 was immunoprecipitated from muscle lysates or after overexpression in HEK cells as described above and specifically eluted using p97 peptides (Abcam, 39788) or FLAG peptides (Sigma, F4799), respectively. Then 20 μL of p97 eluate was added to 30 μL ATPase buffer (50 mM Tris-HCl [pH 8.0], 20 mM $MgCl_2$, 1 mM EDTA, 1 mM DTT, and 3 mM ATP) and incubated for 1 hr at 37°C, and liberated phosphate was measured using Biomol Green assay reagent (Enzo Life Sciences).

Analysis of p97 Hexamer Assembly

To assess p97 hexamer formation, lysates were separated using the NativePAGE Novex Bis-Tris gel system (Invitrogen) according to the manufacturer's instructions. Briefly, muscle or cell lysates were prepared on ice in p97 hexamer buffer (20 mM 4-(2-hydroxyethyl)-1-piperazineethanesulfonic acid (HEPES) [pH 7.2], 0.32 M sucrose, 5 mM $MgCl_2$, 0.2% Nonidet P40, and 2 mM ATP), and 10 μg lysate was mixed with NativePAGE sample buffer (4×) and G-250 sample additive. After gel electrophoresis, the proteins were wet-transferred to PVDF membranes using an X-Cell II blot module (Invitrogen). Proteins were detected as described for immunoblotting. In

parallel, equal amounts of lysate were analyzed by SDS-PAGE and immunoblotting to assess p97 levels.

Immunohistochemistry

Muscles were carefully dissected and snap-frozen in liquid nitrogen-cooled isopentane. Cryosections (10 μm thick) were fixed in cold (−20°C) acetone, washed once with TBS, and then incubated with blocking solution (2% BSA, 5% horse serum, 0.1% Triton in Tris-buffered saline [TBS]) for 1 hr and subsequently with primary antibody at 4°C overnight. The next day, the muscle sections were washed five times with TBS, incubated with fluorescently labeled secondary antibodies for 1 hr, washed five times, and then either mounted or the steps were repeated from blocking onward to co-staining for other proteins. The following antibodies were used: LMNA (Santa Cruz Biotechnology, sc-6215), CaMK2b/g (Thermo Fisher scientific, PA5-36195), DMD (GeneTex, GTX15277), MURF3 (Santa Cruz Biotechnology, sc-166137), MYH4 (Developmental Studies Hybridoma Bank [DSHB], BF-F3), MYH7 (DSHB, BA-F8), MYH2 (DSHB, SC-71), LC3 (CST, 2775), methyl-p97 (Lys315, Merck, ABT286), UNC45B (Eurogentec), and Alexa Fluor secondary antibodies (Invitrogen).

In-Gel Digestion

Preparation of complex muscle lysates for proteomic analysis was performed as described previously (Shevchenko et al., 1996; Lang et al., 2017). Briefly, proteins were separated using 4%–12% Bis-Tris gels (Invitrogen). After Coomassie staining, each lane was cut into ten slices, followed by de-staining of the gel pieces, reduction with 10 mM DTT at 56°C for 45 min, and carbamidomethylation with 55 mM iodoacetamide (IAA) in the dark for 30 min at room temperature. Proteins were digested using the proteases LysC (Wako Pure Chemicals Industries) and trypsin (Promega) overnight at 37°C, the peptides were extracted in acetonitrile, and, after removal of the organic solvent using a SpeedVac concentrator, samples were acidified with trifluoracetic acid and desalted using Stop and Go extraction tips (Rappsilber et al., 2003).

LC-MS/MS Analysis and Data Processing

Proteomic analysis was performed using an Easy nLC 1000 ultra-high performance liquid chromatography (UHPLC) coupled to a QExactive mass spectrometer (Thermo Fisher Scientific) with the previously described settings (Nolte et al., 2014). The raw files were processed using MaxQuant software and its implemented Andromeda search engine (Cox et al., 2011). Parameters were set to default values; Methyl (KR), Dimethyl (KR) and Trimethyl (K) were added as variable modifications for analysis of the methyltransferase assay. For analysis of MYH isoforms, only unique peptides were used for quantification. GO annotations, statistical analysis, and t tests were performed using Perseus software (Tyanova et al., 2016). FDR was calculated by permutation-based approach (number of permutations = 500, fudge factor $[S_0] = 0.1$) (Tusher et al., 2001). For label-free quantification-based proteome analysis of whole soleus muscle, missing values were imputed by a down-shifted normal distribution.

In Vitro Methyltransferase Assay

METTL21C-FLAG (or the mutant GGG construct), overexpressed in HEK cells, and endogenous p97 as a substrate were immunoprecipitated as described above. The beads with the pulled-down substrate were mixed with 2 mM SAM as a methyl group donor and 25 μL methyltransferase buffer (100 mM Tris [pH 8.5], 10 mM $MgCl_2$, and 8 mM DTT), and the volume was adjusted to 50 μL with H_2O. The reaction was initiated by addition of beads carrying immunoprecipitated METTL21C and incubated for 30 min at 37°C. The reaction was terminated by addition of SDS sample buffer, and then the samples were subjected to in-gel digestion and LC-MS/MS.

DATA AND SOFTWARE AVAILABILITY

The accession number for the MS proteomics data reported in this paper is ProteomeXchange Consortium PRIDE partner repository (Vizcaíno et al. 2016): PXD008145.

SUPPLEMENTAL INFORMATION

Supplemental Information includes Supplemental Experimental Procedures, five figures, and five tables and can be found with this article online at https://doi.org/10.1016/j.celrep.2018.03.136.

ACKNOWLEDGMENTS

We acknowledge Sylvia Jeratsch for technical assistance and Kerstin Selbach for helpful comments on this manuscript. We thank Prof. Michael Lammers and Magdalena Kremer for support with the generation of recombinant proteins. We also thank Prof. Thorsten Hoppe and Dr. André Franz for support with plasmids. This work was supported by the DFG Excellence Cluster Cardio-Pulmonary System (ECCPS) and the Cologne Cluster of Excellence on Cellular Stress Responses in Aging-associated Diseases (CECAD) EXC 299/2.

AUTHOR CONTRIBUTIONS

Conceptualization, S.H. and M.K.; Formal Analysis, J.L.W., H.N., and S.H.; Investigation, J.L.W., S.G., T.P., M.B., S.K., and S.H.; Resources, S.G., W.B., N.S., M.S., B.B., T.B., and M.K.; Writing – Original Draft, J.L.W., S.H., and M.K.; Writing – Review & Editing, J.L.W. and M.K.; Visualization, J.L.W. and S.H.; Supervision, S.H. and M.K.; Funding Acquisition, T.B. and M.K.

DECLARATION OF INTERESTS

The authors declare no competing interests.

Received: November 14, 2017
Revised: March 2, 2018
Accepted: March 29, 2018
Published: May 1, 2018

REFERENCES

Blaauw, B., Canato, M., Agatea, L., Toniolo, L., Mammucari, C., Masiero, E., Abraham, R., Sandri, M., Schiaffino, S., and Reggiani, C. (2009). Inducible activation of Akt increases skeletal muscle mass and force without satellite cell activation. FASEB J. *23*, 3896–3905.

Bodine, S.C., Latres, E., Baumhueter, S., Lai, V.K., Nunez, L., Clarke, B.A., Poueymirou, W.T., Panaro, F.J., Na, E., Dharmarajan, K., et al. (2001). Identification of ubiquitin ligases required for skeletal muscle atrophy. Science *294*, 1704–1708.

Buchberger, A., Schindelin, H., and Hänzelmann, P. (2015). Control of p97 function by cofactor binding. FEBS Lett. *589* (*19 Pt A*), 2578–2589.

Ciciliot, S., Rossi, A.C., Dyar, K.A., Blaauw, B., and Schiaffino, S. (2013). Muscle type and fiber type specificity in muscle wasting. Int. J. Biochem. Cell Biol. *45*, 2191–2199.

Clarke, S.G. (2013). Protein methylation at the surface and buried deep: thinking outside the histone box. Trends Biochem. Sci. *38*, 243–252.

Cloutier, P., Lavallée-Adam, M., Faubert, D., Blanchette, M., and Coulombe, B. (2013). A newly uncovered group of distantly related lysine methyltransferases preferentially interact with molecular chaperones to regulate their activity. PLoS Genet. *9*, e1003210.

Cohen, S., Zhai, B., Gygi, S.P., and Goldberg, A.L. (2012). Ubiquitylation by Trim32 causes coupled loss of desmin, Z-bands, and thin filaments in muscle atrophy. J. Cell Biol. *198*, 575–589.

Cohen, S., Nathan, J.A., and Goldberg, A.L. (2015). Muscle wasting in disease: molecular mechanisms and promising therapies. Nat. Rev. Drug Discov. *14*, 58–74.

Cox, J., Neuhauser, N., Michalski, A., Scheltema, R.A., Olsen, J.V., and Mann, M. (2011). Andromeda: a peptide search engine integrated into the MaxQuant environment. J. Proteome Res. *10*, 1794–1805.

Custer, S.K., Neumann, M., Lu, H., Wright, A.C., and Taylor, J.P. (2010). Transgenic mice expressing mutant forms VCP/p97 recapitulate the full spectrum of

IBMPFD including degeneration in muscle, brain and bone. Hum. Mol. Genet. *19*, 1741–1755.

Drexler, H.C., Ruhs, A., Konzer, A., Mendler, L., Bruckskotten, M., Looso, M., Günther, S., Boettger, T., Krüger, M., and Braun, T. (2012). On marathons and Sprints: an integrated quantitative proteomics and transcriptomics analysis of differences between slow and fast muscle fibers. Mol. Cell. Proteomics *11*, M111.010801.

Erce, M.A., Pang, C.N., Hart-Smith, G., and Wilkins, M.R. (2012). The methylproteome and the intracellular methylation network. Proteomics *12*, 564–586.

Frock, R.L., Kudlow, B.A., Evans, A.M., Jameson, S.A., Hauschka, S.D., and Kennedy, B.K. (2006). Lamin A/C and emerin are critical for skeletal muscle satellite cell differentiation. Genes Dev. *20*, 486–500.

Fukuhara, N., Kumamoto, T., and Tsubaki, T. (1980). Rimmed vacuoles. Acta Neuropathol. *51*, 229–235.

Furuno, K., Goodman, M.N., and Goldberg, A.L. (1990). Role of different proteolytic systems in the degradation of muscle proteins during denervation atrophy. J. Biol. Chem. *265*, 8550–8557.

Fusser, M., Kernstock, S., Aileni, V.K., Egge-Jacobsen, W., Falnes, P.O., and Klungland, A. (2015). Lysine Methylation of the Valosin-Containing Protein (VCP) Is Dispensable for Development and Survival of Mice. PLoS ONE *10*, e0141472.

Goldberg, A.L. (1967). Protein synthesis in tonic and phasic skeletal muscles. Nature *216*, 1219–1220.

Hanna, R.A., Quinsay, M.N., Orogo, A.M., Giang, K., Rikka, S., and Gustafsson, A.B. (2012). Microtubule-associated protein 1 light chain 3 (LC3) interacts with Bnip3 protein to selectively remove endoplasmic reticulum and mitochondria via autophagy. J. Biol. Chem. *287*, 19094–19104.

Hartl, F.U., Bracher, A., and Hayer-Hartl, M. (2011). Molecular chaperones in protein folding and proteostasis. Nature *475*, 324–332.

Huang, J., Hsu, Y.H., Mo, C., Abreu, E., Kiel, D.P., Bonewald, L.F., Brotto, M., and Karasik, D. (2014). METTL21C is a potential pleiotropic gene for osteoporosis and sarcopenia acting through the modulation of the NF-κB signaling pathway. J. Bone Miner. Res. *29*, 1531–1540.

Jakobsson, M.E., Moen, A., Bousset, L., Egge-Jacobsen, W., Kernstock, S., Melki, R., and Falnes, P.O. (2013). Identification and characterization of a novel human methyltransferase modulating Hsp70 protein function through lysine methylation. J. Biol. Chem. *288*, 27752–27763.

Janiesch, P.C., Kim, J., Mouysset, J., Barikbin, R., Lochmüller, H., Cassata, G., Krause, S., and Hoppe, T. (2007). The ubiquitin-selective chaperone CDC-48/p97 links myosin assembly to human myopathy. Nat. Cell Biol. *9*, 379–390.

Jentsch, S., and Rumpf, S. (2007). Cdc48 (p97): a "molecular gearbox" in the ubiquitin pathway? Trends Biochem. Sci. *32*, 6–11.

Ju, J.S., Fuentealba, R.A., Miller, S.E., Jackson, E., Piwnica-Worms, D., Baloh, R.H., and Weihl, C.C. (2009). Valosin-containing protein (VCP) is required for autophagy and is disrupted in VCP disease. J. Cell Biol. *187*, 875–888.

Kernstock, S., Davydova, E., Jakobsson, M., Moen, A., Pettersen, S., Mælandsmo, G.M., Egge-Jacobsen, W., and Falnes, P.O. (2012). Lysine methylation of VCP by a member of a novel human protein methyltransferase family. Nat. Commun. *3*, 1038.

Kimonis, V.E., Mehta, S.G., Fulchiero, E.C., Thomasova, D., Pasquali, M., Boycott, K., Neilan, E.G., Kartashov, A., Forman, M.S., Tucker, S., et al. (2008). Clinical studies in familial VCP myopathy associated with Paget disease of bone and frontotemporal dementia. Am. J. Med. Genet. A. *146A*, 745–757.

Klionsky, D.J. (2005). Autophagy. Curr. Biol. *15*, R282–R283.

Kozbial, P.Z., and Mushegian, A.R. (2005). Natural history of S-adenosylmethionine-binding proteins. BMC Struct. Biol. *5*, 19.

Krüger, M., Kratchmarova, I., Blagoev, B., Tseng, Y.H., Kahn, C.R., and Mann, M. (2008). Dissection of the insulin signaling pathway via quantitative phosphoproteomics. Proc. Natl. Acad. Sci. USA *105*, 2451–2456.

Lang, F., Aravamudhan, S., Nolte, H., Türk, C., Hölper, S., Müller, S., Günther, S., Blaauw, B., Braun, T., and Krüger, M. (2017). Dynamic changes in the mouse skeletal muscle proteome during denervation-induced atrophy. Dis. Model. Mech. *10*, 881–896.

Latterich, M., Fröhlich, K.U., and Schekman, R. (1995). Membrane fusion and the cell cycle: Cdc48p participates in the fusion of ER membranes. Cell *82*, 885–893.

Lilienbaum, A. (2013). Relationship between the proteasomal system and autophagy. Int. J. Biochem. Mol. Biol. *4*, 1–26.

Magnani, R., Dirk, L.M., Trievel, R.C., and Houtz, R.L. (2010). Calmodulin methyltransferase is an evolutionarily conserved enzyme that trimethylates Lys-115 in calmodulin. Nat. Commun. *1*, 43.

Malecki, J., Aileni, V.K., Ho, A.Y.Y., Schwarz, J., Moen, A., Sørensen, V., Nilges, B.S., Jakobsson, M.E., Leidel, S.A., and Falnes, P.O. (2017). The novel lysine specific methyltransferase METTL21B affects mRNA translation through inducible and dynamic methylation of Lys-165 in human eukaryotic elongation factor 1 alpha (eEF1A). Nucleic Acids Res. *45*, 4370–4389.

Meyer, H., and Weihl, C.C. (2014). The VCP/p97 system at a glance: connecting cellular function to disease pathogenesis. J. Cell Sci. *127*, 3877–3883.

Nalbandian, A., Ghimbovschi, S., Radom-Aizik, S., Dec, E., Vesa, J., Martin, B., Knoblach, S., Smith, C., Hoffman, E., and Kimonis, V.E. (2012). Global gene profiling of VCP-associated inclusion body myopathy. Clin. Transl. Sci. *5*, 226–234.

Nascimbeni, A.C., Fanin, M., Angelini, C., and Sandri, M. (2017). Autophagy dysregulation in Danon disease. Cell Death Dis. *8*, e2565.

Nishino, I. (2003). Autophagic vacuolar myopathies. Curr. Neurol. Neurosci. Rep. *3*, 64–69.

Niwa, H., Ewens, C.A., Tsang, C., Yeung, H.O., Zhang, X., and Freemont, P.S. (2012). The role of the N-domain in the ATPase activity of the mammalian AAA ATPase p97/VCP. J. Biol. Chem. *287*, 8561–8570.

Nolte, H., Hölper, S., Selbach, M., Braun, T., and Krüger, M. (2014). Assessment of serum protein dynamics by native SILAC flooding (SILflood). Anal. Chem. *86*, 11033–11037.

Perera, S., Holt, M.R., Mankoo, B.S., and Gautel, M. (2011). Developmental regulation of MURF ubiquitin ligases and autophagy proteins nbr1, p62/SQSTM1 and LC3 during cardiac myofibril assembly and turnover. Dev. Biol. *351*, 46–61.

Piccirillo, R., and Goldberg, A.L. (2012). The p97/VCP ATPase is critical in muscle atrophy and the accelerated degradation of muscle proteins. EMBO J. *31*, 3334–3350.

Rappsilber, J., Ishihama, Y., and Mann, M. (2003). Stop and go extraction tips for matrix-assisted laser desorption/ionization, nanoelectrospray, and LC/MS sample pretreatment in proteomics. Anal. Chem. *75*, 663–670.

Rock, K.L., Gramm, C., Rothstein, L., Clark, K., Stein, R., Dick, L., Hwang, D., and Goldberg, A.L. (1994). Inhibitors of the proteasome block the degradation of most cell proteins and the generation of peptides presented on MHC class I molecules. Cell *78*, 761–771.

Sandri, M. (2013). Protein breakdown in muscle wasting: role of autophagy-lysosome and ubiquitin-proteasome. Int. J. Biochem. Cell Biol. *45*, 2121–2129.

Schiaffino, S., and Hanzlíková, V. (1972). Studies on the effect of denervation in developing muscle. II. The lysosomal system. J. Ultrastruct. Res. *39*, 1–14.

Schiaffino, S., and Reggiani, C. (2011). Fiber types in mammalian skeletal muscles. Physiol. Rev. *91*, 1447–1531.

Shevchenko, A., Wilm, M., Vorm, O., Jensen, O.N., Podtelejnikov, A.V., Neubauer, G., Shevchenko, A., Mortensen, P., and Mann, M. (1996). A strategy for identifying gel-separated proteins in sequence databases by MS alone. Biochem. Soc. Trans. *24*, 893–896.

Shi, R.Y., Zhu, S.H., Li, V., Gibson, S.B., Xu, X.S., and Kong, J.M. (2014). BNIP3 interacting with LC3 triggers excessive mitophagy in delayed neuronal death in stroke. CNS Neurosci. Ther. *20*, 1045–1055.

Tanaka, Y., Guhde, G., Suter, A., Eskelinen, E.L., Hartmann, D., Lüllmann-Rauch, R., Janssen, P.M., Blanz, J., von Figura, K., and Saftig, P. (2000). Accumulation of autophagic vacuoles and cardiomyopathy in LAMP-2-deficient mice. Nature *406*, 902–906.

Tresse, E., Salomons, F.A., Vesa, J., Bott, L.C., Kimonis, V., Yao, T.P., Dantuma, N.P., and Taylor, J.P. (2010). VCP/p97 is essential for maturation of ubiquitin-containing autophagosomes and this function is impaired by mutations that cause IBMPFD. Autophagy *6*, 217–227.

Tusher, V.G., Tibshirani, R., and Chu, G. (2001). Significance analysis of microarrays applied to the ionizing radiation response. Proc. Natl. Acad. Sci. USA *98*, 5116–5121.

Tyanova, S., Temu, T., Sinitcyn, P., Carlson, A., Hein, M.Y., Geiger, T., Mann, M., and Cox, J. (2016). The Perseus computational platform for comprehensive analysis of (prote)omics data. Nat. Methods *13*, 731–740.

Vizcaíno, J.A., Csordas, A., Del-Toro, N., Dianes, J.A., Griss, J., Lavidas, I., Mayer, G., Perez-Riverol, Y., Reisinger, F., Ternent, T., et al. (2016). 2016 update of the PRIDE database and its related tools. Nucleic Acids Res. *44*, 11033.

Cell Reports, Volume *23*

Supplemental Information

Skeletal Muscle-Specific Methyltransferase METTL21C Trimethylates p97 and Regulates Autophagy-Associated Protein Breakdown

Janica Lea Wiederstein, Hendrik Nolte, Stefan Günther, Tanja Piller, Martina Baraldo, Sawa Kostin, Wilhelm Bloch, Natalie Schindler, Marco Sandri, Bert Blaauw, Thomas Braun, Soraya Hölper, and Marcus Krüger

Supplemental Information

Supplemental Experimental Procedures

Primer for site directed mutagenesis

Mettl21c inactive mutant (101-108 [LEIGAGAG] to alanine [LEIAAAAA]):

GCTAAAATACTTGAAATTGCTGCTGCAGCAGCCCTTGTTTCC (forward),

GGAAACAAGGGCTGCTGCAGCAGCAATTTCAAGTATTTTAGC (reverse)

p97 K315A:

CCACCTCGCCATGAGTTGCCTCTCTTTTGGGAGCGA

TCGCTCCCAAAAGAGAGGCAACTCATGGCGAGGTGG

Transgenic mouse line

The construct for the targeting vector replacing the *Mettl21c* gene with a LacZ cassette was commercially obtained from Velocigene. After linearization, the construct was transfected into pluripotent embryonal mouse ES cells (F1 hybrid Bl6/129) by electroporation and clones that successfully integrated the construct were selected using G418 antibiotic. ES cells with homologous recombination at the correct locus were injected into C57BL/6 mouse blastocysts and subsequently transplanted into pseudo-pregnant C57BL/6 mice. Resulting chimeras were mated with *Cre*-deleter mice to remove the *loxP* flanked neomycin-resistance cassette. The mice were housed under regular conditions at an ambient temperature of 20-22°C under a 12 hour light/dark cycle, and provided with food and water ad libitum. All animal procedures were performed in accordance with institutional guidelines.

Forced running tests

The forced running exercise was performed on a treadmill (Columbus Instruments) that provides a low-intensity electric shock to the paws of the mouse when the mouse stops running. Mice were trained for two consecutive days while increasing speed from 0 to 12 m/min for a

total duration of 12 min to become familiar with the environment. On the third day, mice were starved for 4 h, and after a 5 min warm-up period, the mice were exercised at 12 m/min for 60 min. Fulfilling any of the three following criteria lead to termination of the exercise session: 1) spending more than 5 consecutive seconds on the shock grid without attempting to re-engage the treadmill, 2) spending more than 50% of time on the shock grid or 3) the mouse was willing to sustain 2 seconds or more of shock for the third time without attempting to re-engage the treadmill. Following the running exercises, mice were returned to their cage and given access to food and water.

In vitro methyltransferase assay with recombinant proteins

Constructs coding for METTL21C with c-terminal 6xHis-Tag (in pET26b vector) and p97 with n-terminal GST-Tag (in pGEX6pi vector) were transformed into E.coli (BL21(DE3)). Expression was induced by addition of 250 mM IPTG and continued o/n at 18°C. Cells were then harvested and lysed. Proteins were purified using an ÄKTA HPLC system with Ni-NTA- or GSH-columns, respectively. Imidazole gradient elution fractions, containing METTL21C-6xHis, were pooled and further purified by Gelfiltration. The GST-tag was removed by incubation with PreScission Protease (GE Healthcare). Successful purification was validated by immunoblotting with METTL21C and p97 antibodies.

In vitro methyltransferase assay was performed in methylation buffer (100 mM Tris pH 8.5, 10 mM MgCl2, 8 mM DTT) with 2 mM S-adenosyl-*L*-methionine for 1h at 37°C. Concentration of recombinant METTL21C ranged from 10 pmol to 1 nmol. Methylation was analyzed by mass spectrometry and immunoblotting with antibodies raised against mono, di- and trimethylated lysine, as well as the p97-K315 specific trimethyl antibody.

Size exclusion chromatography

Cells were lysed in ice-cold size exclusion chromatography (SEC) buffer (50 mM KCl, 50 mM sodium acetate, pH 7.2), supplemented with protease and phosphatase inhibitor cocktail and sonicated. The cleared lysate was concentrated using 10K Amicon filters. Gel filtration was performed on a BioSep 5 µm SEC column (LC Column, 300 × 4.6 mm, Phenomenex) at a flow rate of 0.3 mL/min at 12°C, and fractions were collected every minute.

Figure S1

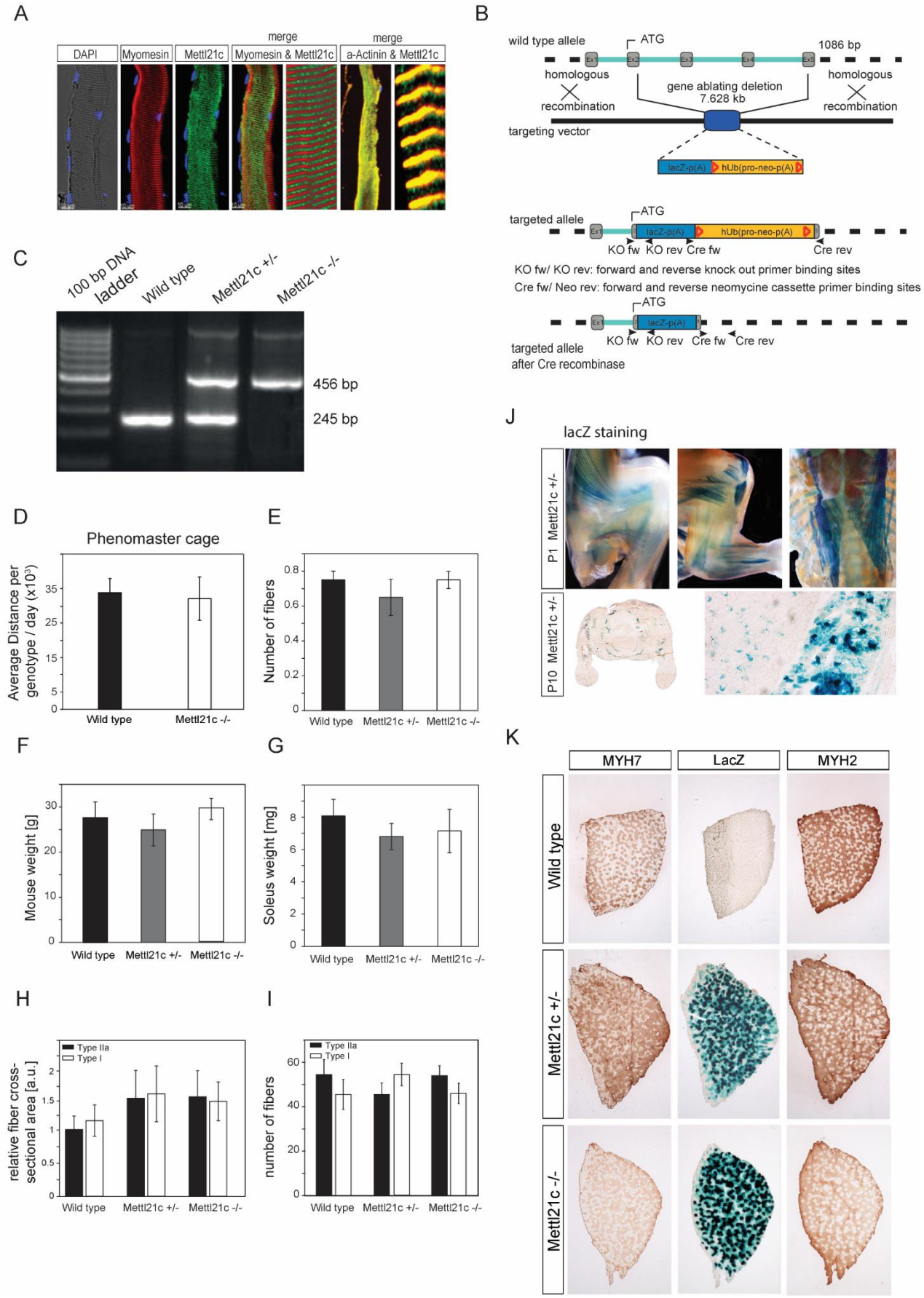
A
DAPI
Myomesin
Mettl21c
merge
Myomesin & Mettl21c
merge
a-Actinin & Mettl21c
B
wild type allele
ATG
1086 bp
homologous recombination
gene ablating deletion 7.628 kb
homologous recombination
targeting vector
lacZ-p(A)
hUb(pro-neo-p(A)
targeted allele
KO fw
KO rev
Cre fw
Cre rev
KO fw/ KO rev: forward and reverse knock out primer binding sites
Cre fw/ Neo rev: forward and reverse neomycine cassette primer binding sites
targeted allele after Cre recombinase
C
100 bp DNA ladder
Wild type
Mettl21c +/-
Mettl21c -/-
456 bp
245 bp
D
Phenomaster cage
Average Distance per genotype / day (x10³)
Wild type
Mettl21c -/-
E
Number of fibers
Wild type
Mettl21c +/-
Mettl21c -/-
F
Mouse weight [g]
G
Soleus weight [mg]
H
relative fiber cross-sectional area [a.u.]
Type IIa
Type I
I
number of fibers
J
lacZ staining
P1 Mettl21c +/-
P10 Mettl21c +/-
K
MYH7
LacZ
MYH2
Wild type
Mettl21c +/-
Mettl21c -/-

Figure S1: Genetic ablation of *Mettl21c* by homologous recombination and tissue-specific detection of lacZ reporter. Related to Figure 1 (**A**) Immunostaining for METTL21C in human longitudinal muscle sections, with co-staining for the Z-disk marker α-actinin-2 and M-band marker myomesin-2. DAPI (blue) was used to counterstain nuclei; scale bars = 10 µm. (**B**) Targeted disruption of the *Mettl21c* genomic locus. Schematic representation of the *Mettl21c* locus (wild-type allele), the targeting vector, and the disrupted allele produced by homologous recombination. Insertion of the β-galactosidase cassette and neomycin resistance gene deleted the coding sequence from exon 2 to exon 5. The targeting vector introduces two *loxP* sites flanking the selection cassette and was deleted by crossing to a *cre*-recombinase expressing mouse strain. (**C**) PCR amplification of genomic DNA from the *Mettl21c* gene locus to genotype mice. (**D-I**) Various parameters were determined for mice that participated in voluntary and forced running experiments, including (D) average distance moved by wild-type and *Mettl21c*$^{-/-}$ mice in a phenomaster cage, (E) soleus fiber length, (F) mouse weight, (G) soleus weight, (H) relative fiber area, (I) and relative number of type I and type IIa fibers in the soleus of wild-type and *Mettl21c*$^{-/-}$ mutants per 100 fibers. All data in D-I are mean ± SD (n = 3). (**J**) β-galactosidase staining of *Mettl21*$^{+/-}$ mice during the early postnatal stages. (**K**) Immunohistochemical staining of consecutive sections from wild-type, *Mettl21*$^{+/-}$ and *Mettl21c*$^{-/-}$ soleus muscle using MYH7 (left), β-galactosidase (middle) and MYH2 (right).

Figure S2

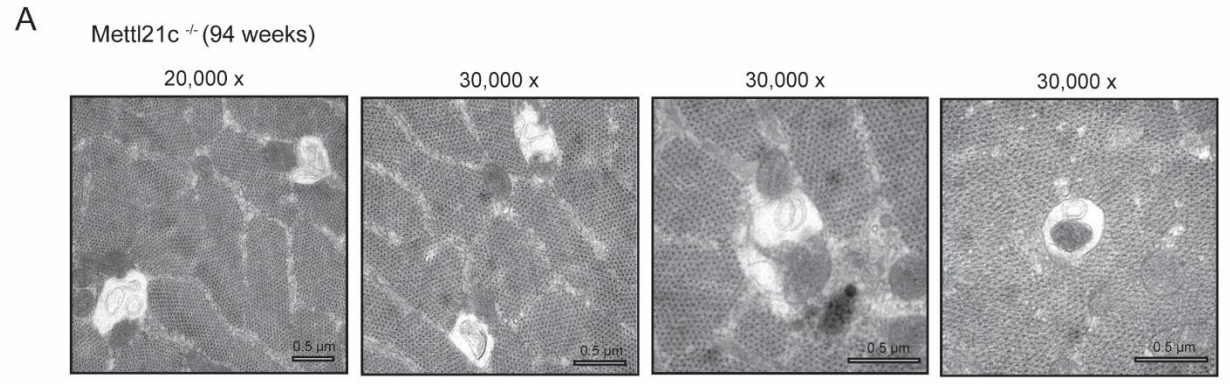

Figure S2: Electron microscopy reveals accumulation of autophagic vacuoles in the soleus of *Mettl21c*$^{-/-}$ mice. Related to Figure 2. (**A**) Representative electron micrographs of the soleus from 94-week-old *Mettl21c*$^{-/-}$ mutants showing non-digested autophagosomes.

Figure S3

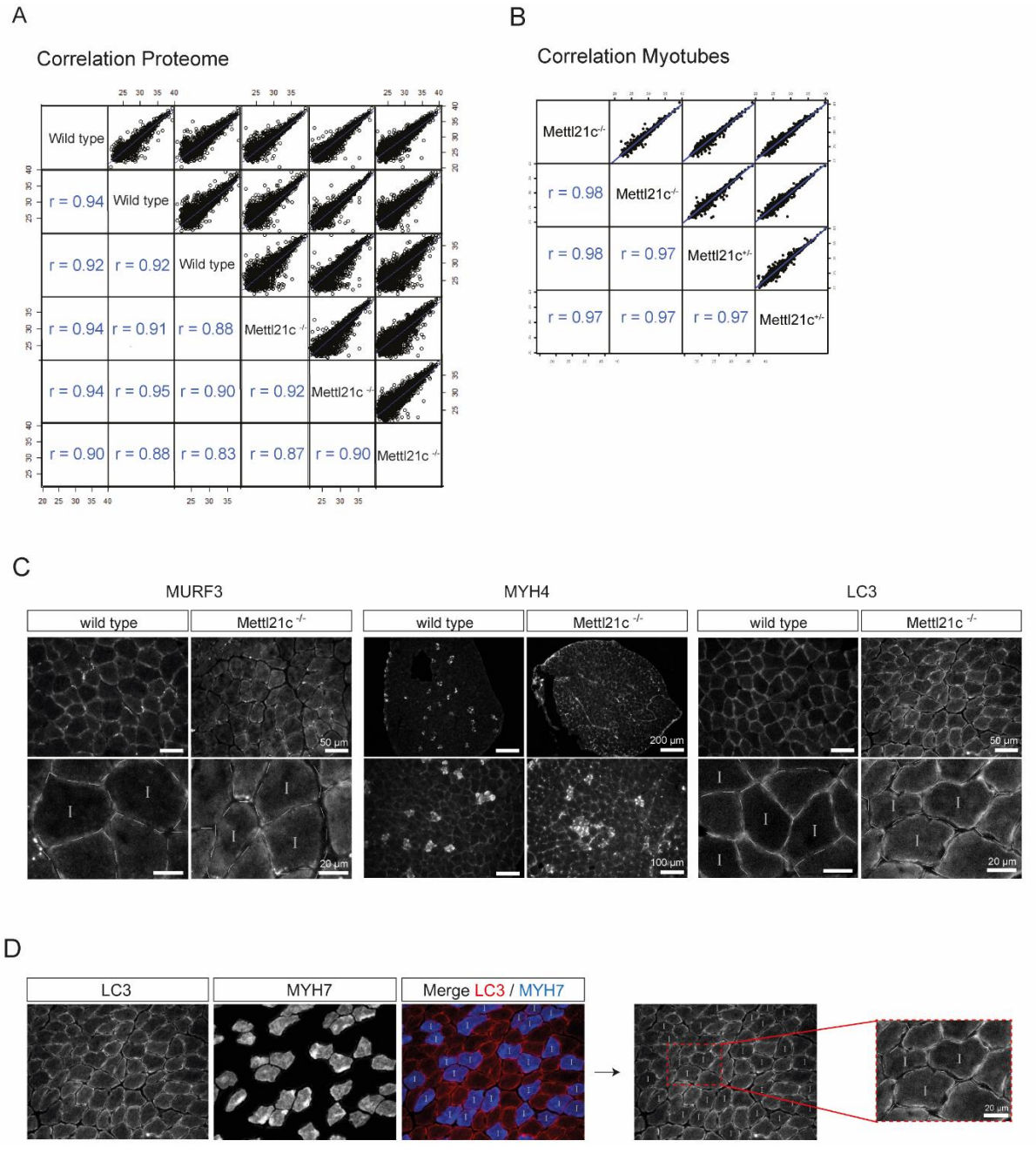

Figure S3: Correlation of muscle proteomes and immunohistochemistry of proteins with enhanced levels in *Mettl21c*$^{-/-}$ mutants. Related to Figure 3. (**A**) Correlation of $\log_2$ protein intensities for *Mettl21*$^{-/-}$ and control wild-type whole soleus muscles. (**B**) Correlation of $\log_2$ protein intensities for isolated β-galactosidase-positive muscle fibers from *Mettl21c*$^{+/-}$ and *Mettl21c*$^{-/-}$ mutants. (**C**) Immunostaining for TRIM54, MYH4 and LC3 in soleus cryosections.

(**D**) Workflow example for fiber type characterization based on co-staining with the MYH7 antibody. Slow type I fibers (blue) are marked with “I”.

Figure S4

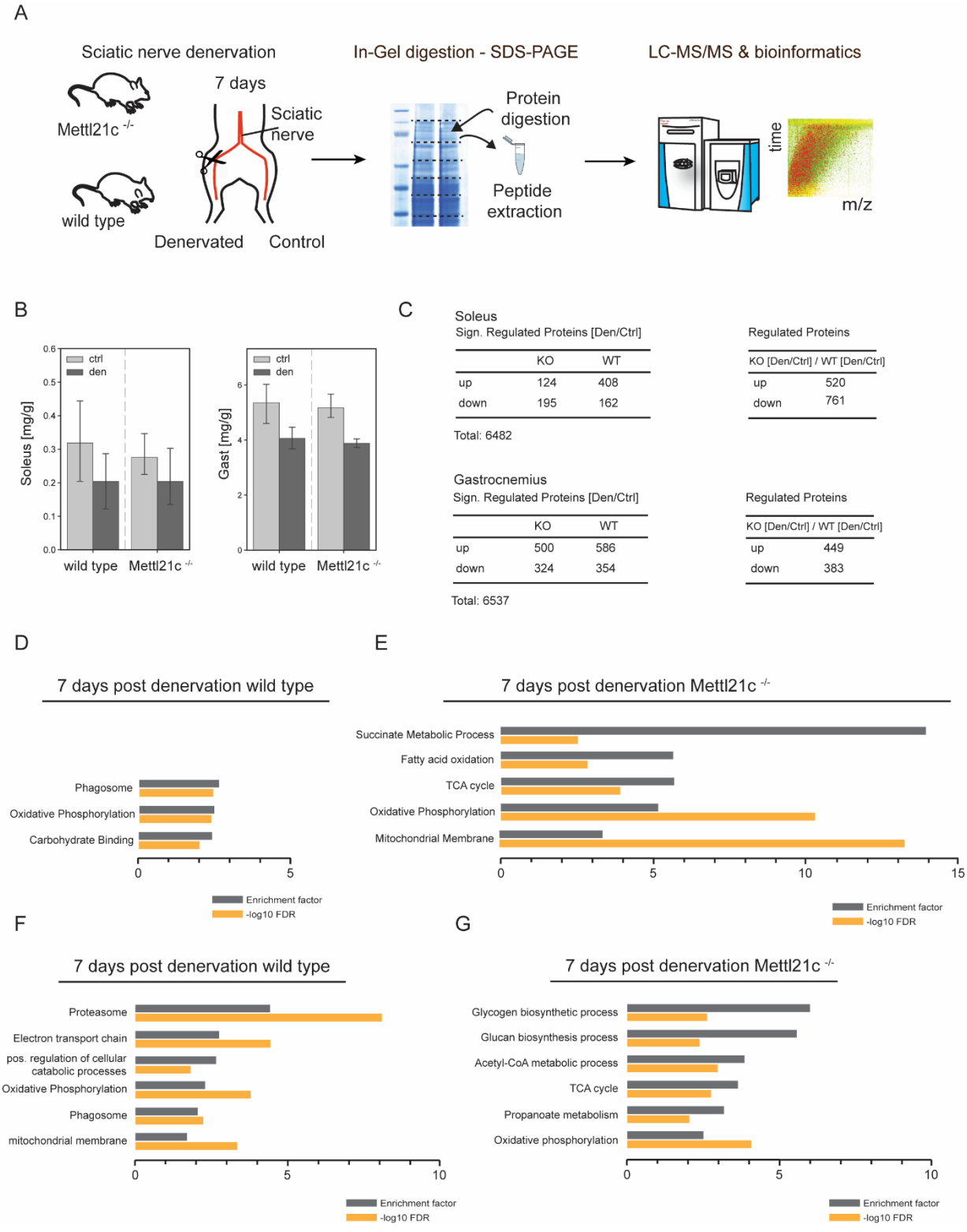

Figure S4: Experimental workflow for the sciatic nerve denervation experiments and evaluation of MS data. Related to Figure 4. (**A**) Schematic illustration of denervation of the sciatic nerve and the proteomic workflow. Unilateral denervation via sciatic nerve section was

performed; after seven days, the animals were sacrificed and muscles dissected for analysis. The contralateral hind limb served as a control. **(B)** Weight of muscles from denervated (den) and control (ctrl) legs in relation to total body weight at 7 days after denervation for wild-type and *Mettl21c*$^{-/-}$ mice. Data are mean ± SD (n = 3). **(C)** Table of the numbers of regulated proteins (t-test significant after permutation-based FDR cutoff of 0.05) in wild-type and *Mettl21c*$^{-/-}$ soleus and GAST at 7 days after denervation (left panel). The $\log_2$ fold changes (den/ctrl) were compared between wild-type and *Mettl21c*$^{-/-}$ mice and the number of differentially regulated proteins ($\log_2$ fold change > 0.58) was determined (right panel). **(D-G)** Fisher exact tests of enriched GO annotations in wild-type and *Mettl21c*$^{-/-}$ soleus (D, E) and GAST at 7 days after denervation **(**F, G**)**.

Figure S5

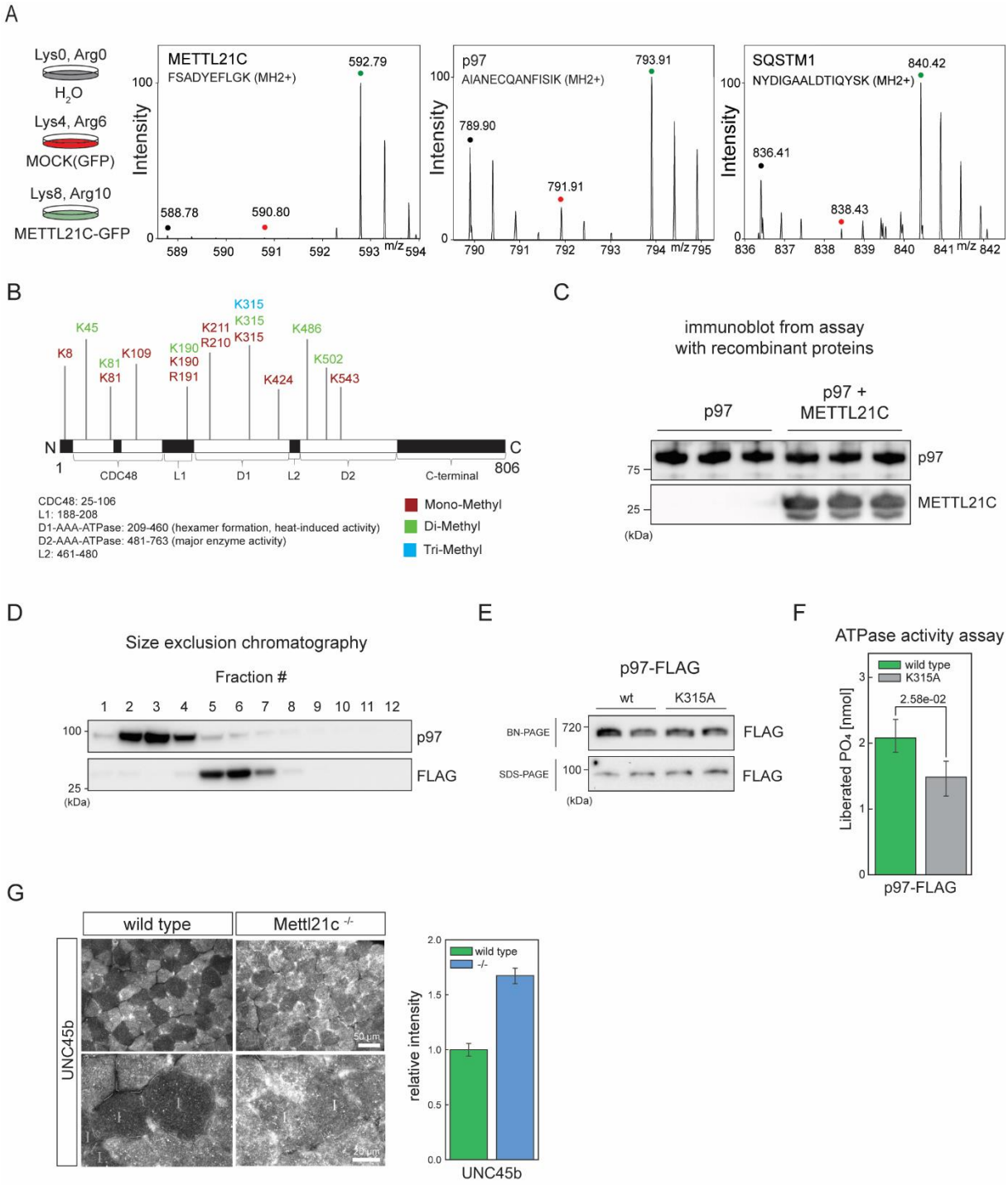

Figure S5: Overview of immunoprecipitation experiments, p97 methylation sites, size exclusion chromatography, p97 hexamer assembly and activity. **Related to Figure 5.** (**A**) Triple SILAC labeling of 293 HEK cells. Control transfection with H_2O (light = Lys0, Arg0), the GFP expression vector (middle = Lys4, Arg6) or Mettl21c-GFP expression construct (heavy = Arg10, Lys8). After immunoprecipitation with GFP-beads, the three samples were mixed in

a 1:1:1 ratio and analyzed by mass spectrometry. Representative SILAC pairs are shown for peptides from METTL21C (left panel), p97 (middle panel) and p62 (right panel). (**B**) Methylation sites identified on p97 after incubation with METTL21C. (**C**) Immunoblot of recombinant p97 and METTL21C proteins utilized for in vitro methylation assay. (**D**) Immunoblotting of p97 and METTL21C-FLAG from HEK cell lysates fractionated by size exclusion chromatography. (**E**) BN-PAGE and SDS-PAGE of HEK lysates after expression of p97 wild type or K315A FLAG-fusion using anti-FLAG antibody for detection. SDS-PAGE is used for determination of total p97 levels and serves as loading control. (**F**) Bar plot of ATPase activity assay. p97 wild type and K315A FLAG-fusion were overexpressed in HEK cells and pulled down with FLAG beads. Levels of liberated phosphate after 1 hour of incubation were determined using a malachite green-based colorimetric assay. Bar plots represent mean ± 0.95 CI (n = 4). (**G**) Immunostaining of UNC45b and quantitative analysis of fluorescent signals in slow type I fibers. Slow fibers were identified by co-staining with MYH7. Bar plots represent mean ± 0.95 CI (n = 15-20).